Supplementary Data

Facile synthesis of novel NNO tethered copper(II) complexes: Characterization details, theoretical studies, promising enzyme-like activities and bio-molecular interactions

Subrata Mandal, Rahul Naskar, Apurba Sau Mondal, Biswajit Bera and Tapan K. Mondal*

Department of Chemistry, Inorganic Section, Jadavpur University, Kolkata 700 032, India

e-mail: tapank.mondal@jadavpuruniversity.in

---

1. Experimental and Computational Details

1.1. Materials and methods

2,4-di-tertbutyl phenol, 8-aminoquinoline and copper(II) perchlorate hexahydrate were purchased from Sigma Aldrich. 3,5-di-tertbutylsalicylaldehyde were prepared from 2,4-di-tertbutyl phenol by following Duff's method.[1] All other chemicals and solvents were reagent grade, purchased from commercial sources and were used without further purification.

Elemental analyses (C, H and N) were performed using a PerkinElmer Series-II CHN-2400 CHNS/O elemental analyzer. Electronic spectra were taken in acetonitrile and DMSO on a Lambda 750 PerkinElmer spectrophotometer at room temperature (298 K). Luminescence properties were observed by Shimadzu RF-6000 fluorescence spectrophotometer at room temperature (298 K). IR spectra were recorded as KBr pellets on a RX-1 PerkinElmer spectrometer operating from 4000-400 cm^{-1}. HRMS mass spectra were obtained on a Waters (Xevo G2 Q-TOF)

mass spectrometer in acetonitrile medium. A JENCONS 4010 Conductivity Meter was used to measure the conductance. The X-band EPR spectra were measured in anhydrous DCM medium at room temperature (at 298 K) on a Magnettech GmbH MiniScope MS400 spectrometer (equipped with temperature controller TC H03), where the microwave frequency was measured with an FC400 frequency counter. Viscometric measurements were performed using an Ostwald viscometer placing it in a thermostated water bath at 25.0 °C. Flow time was measured with a digital stopwatch. Luminescence lifetime measurements were carried out by using time-correlated single photon counting set up from Horiba Jobin-Yvon. The luminescence decay data were collected on a Hamamatsu MCP photomultiplier (R3809) and were analyzed by using IBH DAS6 software. Circular dichroism (CD) studies were made on a JASCO spectropolarimeter (model J815, Jasco International Co., Japan) equipped with a thermalprogrammer (model PFD–425L/15) and temperature controller using a 1 cm path length rectangular quartz cuvette.

Caution! *Metal complexes containing organic ligands in the presence of perchlorate and azides are potentially explosive. For safety purpose, one should prepare very little amount of compound and handle it cautiously. In our case, no problems were experienced during working with the same salts.*

1.2 Synthesis of Cu (II) complexes [Cu(L)(NCS)] (1), [Cu(L)(N_3)] (2) and [Cu(L)(NO_3)] (3)

The tridentate Schiff base ligand **LH** was prepared from 3,5-dimethylsalicylaldehyde and 8-aminoquinoline according to the procedure reported.[2]

Complex **[Cu(L)(NCS)] (1)** was synthesized by drop wise addition of a methanolic solution of **LH** (0.181 g, 0.5 mmol) to an aqueous solution of Copper(II) perchlorate hexahydrate (0.185 g, 0.067 mmol) and ammonium thiocyanate (NH_4SCN) (0.075 g, 1 mmol) with constant stirring. The

resulting mixture was stirred for 5 h at room temperature. The solution was filtered and kept undisturbed in open air at room temperature for slow evaporation. After several days, green crystals suitable for X-ray crystallography were obtained. Yield, 0.157 g (68%).

Anal. Calc. for $C_{25}H_{27}CuN_3OS$: C, 62.41; H, 5.66; N, 8.73. Found: C, 62.22; H, 5.45; N, 8.61. IR (KBr, cm^{-1}): 2960.31 υ(C-H); 2042.41 υ(C=N of –N=C=S); 1600.20 υ(C=N for imine of Schiff base). HRMS: Calculated for $C_{24}H_{27}CuN_2O$ **[Cu(L)]**$^+$ ion (m/z): 422.1419; found: 422.1393. Molar conductance (Λ_m) in DMSO: 3.2 $\Omega^{-1}cm^2mol^{-1}$. UV-Vis (in DMSO), λ_{max} (ε, $M^{-1}cm^{-1}$): 470 (16419.159), 362 (17460.425), 344 (23790.229), 328 (22214.628), 290 (17871.452).

Complex, **[Cu(L)(N_3)] (2)** was prepared by a procedure similar to that given in the case of **1**, but adding sodium azide (NaN_3) instead of NH_4SCN to the reaction mixture. Pale yellow block crystals suitable for X-ray diffraction were obtained by gradual evaporation of the filtrate after two weeks. Yield was 0.2425 g (65%).

Anal. Calc. for $C_{24}H_{27}CuN_5O$: C, 61.98; H, 5.85; N, 15.06. Found: C, 61.77; H, 5.72; N, 14.82. IR (KBr, cm^{-1}): 2955.26 υ(C-H); 2041.53 υ(N=N of $–N_3$); 1598.59 υ(C=N for imine of Schiff base). HRMS: Calculated for $C_{24}H_{27}CuN_2O$ **[Cu(L)]**$^+$ ion (m/z): 422.1419; found: 422.1393. Molar conductance (Λ_m) in DMSO: 3.5 $\Omega^{-1}cm^2mol^{-1}$. UV-Vis (in DMSO), λ_{max} (ε, $M^{-1}cm^{-1}$): 471 (16898.69), 362 (18693.504), 345 (25502.838), 330 (25160.316).

Complex **[Cu(L)(NO_3)] (3)** was synthesized by mixing equimolar amounts of the ligand **LH** (0.181 g, 0.5 mmol) and $Cu(NO_3)_2$•$3H_2O$ (0.126 g, 0.5 mmol) in methanol (15 mL). After stirring for 5-6 h at room temperature the reaction mixture was filtered and allowed for evaporation which ultimately produced green crystal. Yield, 0.169 g (70%).

Anal. Calc. for $C_{24}H_{27}CuN_3O_4$: C, 59.43; H, 5.61; N, 8.66. Found: C, 59.17; H, 5.51; N, 8.45. IR (KBr, cm^{-1}): 2957.89 υ(C-H); 1603.63 υ(C=N for imine of Schiff base). HRMS: Calculated for $C_{24}H_{27}CuN_2O$ **[Cu(L)]**$^+$ ion (m/z): 422.1419; found: 422.1393. Molar conductance (Λ_m) in DMSO: 3.4 $\Omega^{-1}cm^2mol^{-1}$. UV-Vis (in DMSO), λ_{max} (ε, $M^{-1}cm^{-1}$): 470 (22118.722), 363 (25982.369), 346 (33120.524), 290 (24762.991).

1.3 X-ray crystallographic study

Suitable single crystals of complexes **1**, **2** and **3** were mounted on a glass fibre, and diffraction intensities were measured at 293˚C with an automated Bruker SMART APEX CCD diffractometer using graphite monochromatized Mo-Kα radiation (λ = 0.71073 Å). Reflection data were recorded using the ω scan technique and the data were reduced and integrated through SAINT[5] program and corrected for Lorentz and polarization effects. A multi-scan absorption correction was made with SADABS.[6] The crystal structures were solved by direct methods and refined by full-matrix least-squares refinements on F^2 using SHELXL-2016/6 program[4] implemented in WinGX system.[3] All non-hydrogen atoms were refined anisotropically. Positions of hydrogen atoms were generated using SHELXL and treated as riding model. Details of crystal analysis, data collection and structure refinement are given in Table S1. Molecular structures of the crystals were drawn with ORTEP-32.[7]

1.4 Theoretical calculations

All computations were performed using the GAUSSIAN09 program package[8] with the aid of the GaussView, Version 5 visualization program.[9] Full geometry optimizations for the ground state of the ligands and the Cu(II)-complexes were carried out using density functional theory (DFT) method at the B3LYP level.[10] In the calculation, 6-31G (d-p) basis set was assigned to all the

elements (C, H, N and O) excluding copper for which the Los Alamos effective core potentials plus the Double Zeta (LanL2DZ) basis set were employed.[11] The vibrational frequency calculations were performed on the optimized geometries to assure that each configuration represents a local minima associated with positive eigen values only on the potential energy surface. The absorbance spectral properties of the complexes in DMSO medium were calculated by Time-dependent density functional theory (TDDFT)[12] formalism using conductor-like polarizable continuum model (CPCM).[13] Fractional contributions of various groups or atoms to each molecular orbital were computed by GaussSum program.[14] Calculated coordination geometries of complex **1**, **2** and **3** are shown in Table S2.

2. *Hirshfeld Surface Analysis* of complexes 1, 2 and 3

In order to visualize the intermolecular interactions, prevailing in the crystal, Molecular Hirshfeld surfaces (HS)[15] and the associated 2D-fingerprint[16] plots of **1-3** were calculated using ***Crystal Explorer 17.5*** software.[17] Bond lengths to hydrogen atoms were automatically set to standard values, while the structural input CIF. files of the crystals **1-3** were read into the software for calculations.

For each point on the Hirshfeld isosurface, two distances d_e, the distance from the point to the nearest nucleus external to the surface and d_i, the distance to the nearest nucleus internal to the surface, are defined. The normalized contact distance (d_{norm}) based on d_e and di is given by equ (1)

$$d_{norm} = \frac{(d_i - r_i^{vdw})}{r_i^{vdw}} + \frac{(d_e - r_e^{vdw})}{r_e^{vdw}} \quad (1)$$

where, r_i^{vdW} and r_e^{vdW} are the van der Waals radii of the atoms. The value of d_{norm} is negative or positive depending on intermolecular contacts being shorter or longer than the van der Waals separations.

Graphical plots of the molecular Hirshfeld surfaces mapped with d_{norm} uses a red-white-blue colour scheme, where bright red spots highlight shorter contacts, white areas represent contacts around the van der Waals separation, and blue regions are devoid of close contacts. To visualize the molecular moiety, transparent mapped surfaces are usually shown. For a given crystal structure and set of spherical atomic electron densities, the Hirshfeld surface is unique and thus it suggests the possibility of gaining additional insight into the intermolecular interaction of molecular crystals. 2D Fingerprint plot resolved into different contacts contributed to the total Hirshfeld surface area of the complex **1**, complex **2** and complex **3**.

3. Enzyme-like activities of complexes 1, 2 and 3.

3.1 Catecholase activity

Catalytic activity of the present mononuclear Cu(II) complexes **1**, **2** and **3** towards the aerial oxidation of the substrate 3,5-ditert-butyl catechol (3,5-DTBC) to 3,5-di-tert-butyl-o-quinone (3,5-DTBQ) was explored spectrophotometrically under aerobic conditions at 298K. The kinetic parameters were estimated by capturing the steady growth of characteristic absorption intensity around 400 nm which corresponds to the oxidation product 3,5-DTBQ. Because the substrate, complexes, and their products are extremely soluble in acetonitrile, all of the studies were carried out in this medium. In all experiments, 10^{-4} (M) solution of each complex (**1**, **2** and **3)** was reacted with at least 100-fold more concentrated substrate to maintain pseudo-first order reaction conditions.[18] The rate of a reaction was determined from the initial rate method and catalytic rate constant values were evaluated applying Michaelis–Menten enzyme kinetics and Lineweaver–

Burk double reciprocal plots.[19] Blank experiments without catalyst (complex) were also performed under identical conditions to discard the phenomenon of auto-oxidation of the substrate by air.

3.2 Phenoxazinone synthase like activity

Using *o*-aminophenol (OAPH) as a model substrate, phenoxazinone synthase mimicking activity of **1**, **2** and **3** was investigated using a similar approach as stated above. The rise of the oxidation product 2-aminophenoxazine-3-one at λmax ~ 436 nm was used to monitor the processes spectroscopically. In this study 10^{-4} M solutions of complexes were used.

3.3 Rationalization of kinetic parameters

The kinetics of 3,5-DTBC (or OAPH) oxidation to 3,5-DTBQ (or APX) catalysed by **1**, **2** or **3** were estimated using the initial rate method, recording the amplification of 400 nm (or 436 nm) absorption intensity at 298K. For a set of catalyst–substrate concentration, the rate constant was calculated by plotting ΔA (change in absorbance) vs. t (time) at 400 nm (catecholase) or 436 nm (phenoxazinone synthase). The conversion of the reaction rate units from ΔA/s to M/s was done using ε value 1500 $M^{-1}cm^{-1}$ (for DTBQ)[19b] and 18300 $M^{-1}cm^{-1}$ (for APX).[19c-d]

One demo calculation of catecholase activity of complex **1** was demonstrated below:

1×10^{-4} (M) acetonitrile solution of complex **1** was mixed with 1×10^{-2} (M) solution of 3,5-DTBC in acetonitrile at 298K under aerobic conditions. The concentration of the catalyst as well as the substrate are halved after mixing; i.e [catalyst] = 5×10^{-5} (M) and [DTBC] = 5×10^{-3} (M).

Slope of "ΔA (change in absorbance at 400 nm) vs. t (time)" plot = Rate $(\frac{dA}{dt})$ = 0.04005 min^{-1} (See Fig. S22).

Rate $(V) = \frac{1}{\varepsilon L} \times \frac{dA}{dt} = \frac{0.04005\ min^{-1}}{(1500 M^{-1} cm^{-1}) \times 1cm} = 2.67 \times 10^{-5}\ M.min^{-1}$

So, at $[DTBC] = 5 \times 10^{-3}\ M; V = 2.67 \times 10^{-5}\ M.min^{-1}$

$\frac{1}{DTBC} = 200\ M^{-1}; \frac{1}{V} = 3.75 \times 10^{4}\ M^{-1}.min$

Now keeping the catalyst (here **1**) concentration constant (5×10^{-5} M), the substrate (3, 5-DTBC) concentration was varied from 10^{-3} (M) to 10^{-2} (M) to explore the rate dependence on the substrate concentration. Lineweaver–Burk (double reciprocal) plot was constructed to extract all the kinetic parameters, such as the maximum initial reaction rate (V_{max}), Michaelis–Menten binding constant (K_M) and turnover numbers (K_{cat}) which are shown below:

$V_{max} = 4.1099 \times 10^{-5}\ M.min^{-1}$

$K_M = 2.869539 \times 10^{-3}\ M$

$K_{cat} = \frac{V_{max}}{C_0} = \frac{4.1099 \times 10^{-5}\ M.min^{-1}}{5 \times 10^{-5}\ M} = 8.22 \times 10^{-1}\ min^{-1} = 49.3\ h^{-1}$

One demo calculation of phenoxazinone synthase mimicking activity of complex **1** was demonstrated below:

1×10^{-4} (M) acetonitrile solution of complex **1** was mixed with 1×10^{-2} (M) solution of OAPH in acetonitrile at 298K under aerobic conditions. The concentration of the catalyst as well as the substrate are halved after mixing; i.e [catalyst] = 5×10^{-5} (M) and [OAPH] = 5×10^{-3} (M).

Slope of "ΔA (change in absorbance at 436 nm) vs. *t* (time)" plot = Rate $(\frac{dA}{dt})$ = 0.00138 min^{-1} (See Fig. S23).

Rate $$(V) = \frac{1}{\varepsilon L} \times \frac{dA}{dt} = \frac{0.00138\, min^{-1}}{(18300 M^{-1} cm^{-1}) \times 1cm} = 7.54 \times 10^{-8}\, M.min^{-1}$$

So, at $$[OAPH] = 5 \times 10^{-3}\, M;\ V = 7.54 \times 10^{-8}\, M.min^{-1}$$

$$\frac{1}{DTBC} = 200\, M^{-1};\ \frac{1}{V} = 1.33 \times 10^{7}\, M^{-1}.min$$

Now keeping the catalyst (here **1**) concentration constant (5×10^{-5} M), the substrate (OAPH) concentration was varied from 10^{-3} (M) to 10^{-2} (M) to explore the rate dependence on the substrate concentration. Lineweaver–Burk (double reciprocal) plot was constructed to extract all the kinetic parameters, such as the maximum initial reaction rate (V_{max}), Michaelis–Menten binding constant (K_M) and turnover numbers (K_{cat}) which are shown below:

$$V_{max} = 1.18002 \times 10^{-7}\, M.min^{-1}$$

$$K_M = 2.974329 \times 10^{-3}\, M$$

$$K_{cat} = \frac{V_{max}}{C_0} = \frac{1.18002 \times 10^{-7}\, M.min^{-1}}{5 \times 10^{-5}\, M} = 2.36 \times 10^{-3}\, min^{-1} = 1.42 \times 10^{-1}\, h^{-1}$$

3.4 Detection of hydrogen peroxide in the course of catalysis

The involvement of atmospheric oxygen in the oxidation of DTBC (catecholase activity) or OAPH (phenoxazinone synthase mimicking activity) was confirmed from the detection of hydrogen peroxide in the reaction mixture with reported literature.[20] In the course of oxidation of DTBC or OAPH in acetonitrile, H_2SO_4 was added to the reaction mixture to bring it to pH 2. After a given amount of time had passed, an equivalent volume of water was added to prevent further oxidation. The oxidation product, o-quinone or phenoxazinone species were extracted using DCM as an extractant. The aqueous layer was then injected with a 10% KI solution (1 mL) and a 3% ammonium molybdate solution. A spectrophotometer was used to track the development of I_3^- species at λ_{max} = 353 nm, which could be related to hydrogen peroxide production in the course of catalytic oxidation. Since atmospheric dioxygen can oxidize I^-, blank experiments (without catalyst or without substrates) were also performed. However, only very minor formation of the I_3^- band was observed during the blank test.

4. DNA-binding studies

4.1 Absorption spectral studies

The binding experiments of metal complexes with calf thymus (CT) DNA were performed in Tris HCl/50 mM NaCl buffer (pH 7.4). A stock solution of CT DNA was prepared in that buffer

and the concentration of the CT DNA was determined by dividing its absorption value at 260 nm with the molar extinction coefficient value i.e. 6600 M^{-1} cm^{-1}.[21] It was stored at 4°C and used within one week. The stock solution of the complexes **1**–**3** was prepared in 1:10 DMSO /buffer medium and was suitably diluted with Tris buffer whenever necessary. This low DMSO percentage added to the DNA solution should not interfere with the nucleic acid.[22] 2 ml of 10 μM solution of each complex was taken in a cuvette and absorption titration was carried out by gradually adding the CT DNA solution to it until saturation occurred. After each addition, the solution was stirred homogeneously and let to equilibrate for 4 min before collecting the absorption profile.

4.2 Fluorescence spectral studies

The ability of the synthesized complex (**1**, **2** and **3**) to dislocate 3,8-diamino-5- ethyl-6-phenylphenanthridinium bromide (EB) from its EB-DNA complex was studied by the fluorescence titration method. 30 μM CT DNA in Tris– HCl/NaCl buffer solution (pH 7.4) was pretreated with 15 μM EB to prepare the CT DNA–EB complex, which produced an enhanced fluorescence emission at 608 nm when excited at 540 nm. Quenching of that emission was monitored with the subsequent addition of **1**, **2** and **3**.

4.3 Viscometric measurements

The viscosity of the CT-DNA solutions (34.8μM) was measured in the presence of increasing amounts of the complexes using an Ostwald viscometer placing it in a thermostated water bath at 25.0 °C. Flow time was measured with a digital stopwatch and each sample was measured three times, then the average flow time was calculated. Viscosity values were calculated from the observed flow time of DNA-containing solutions (t) corrected for the flow time of buffer alone

(t_0), $\eta = t - t_0$. The data is reported as $(\eta / \eta_0)^{1/3}$ versus the ratio of the concentration of the compound to CT-DNA (R = [compound]/[CT-DNA]), where η is the viscosity of CT-DNA in the presence of the compound and η_0 is the viscosity of CT-DNA solution alone.[23]

5. Methods for BSA-interaction studies

The binding interaction between BSA and Cu(II) complexes (**1, 2** and **3**) were deciphered by employing UV-Vis and fluorescence methods. A stock solution of BSA was prepared using 500 mM phosphate buffer saline (PBS) at pH 7.4 and stored in the dark at 4°C for further use. BSA concentration was measured by taking absorbance at 280 nm in UV-Vis spectra (molar extinction coefficient 66,400 dm^3 mol^{-1} cm^{-1}).[24] The stock solution of **1, 2** and **3** were prepared in DMSO medium. For recording UV-Vis spectra, BSA-concentration was kept constant (10 μM) while varying the concentration of the complex added to it. In fluorescence experiment, tryptophan fluorescence of BSA was recorded in the range 290–500 nm at an excitation wavelength of 280 nm using a slit width of 10 nm. Quenching of emission intensity at ~335 nm for BSA was monitored with subsequent addition of metal complex. Synchronous fluorescence spectra (SFS) were also captured in the same instrument in the range of 250–320 nm by scanning the excitation and emission monochromator simultaneously. Different wavelength interval ($\Delta\lambda = \lambda_{em} - \lambda_{ex}$) of $\Delta\lambda$ = 15 nm and $\Delta\lambda$ =60 nm were set to observe the spectrum behavior of tyrosine and tryptophan residues of BSA, respectively. All fluorescence intensity data was inner filter effects corrected employing the equ (2)[25]

$$F_{cor} = F_{obsexp} [(A_{ex}+A_{em})/2] \qquad (2)$$

where F_{cor} and F_{obsexp} are the fluorescence intensity corrected and observed experimentally, respectively, and A_{ex} and A_{em} are the sum of the absorbance of BSA and the copper(II) complex at excitation and emission wavelengths, respectively.

6. Circular dichroism measurements

Circular dichroism (CD) spectra were obtained employing JASCO (J-815) spectropolarimeter at 298 K using a quartz cuvette of 1 cm cell path length. The spectra were recorded in far UV region (200–260 nm) for BSA in presence and absence of copper complexes **1**-**3**. Concentration of BSA was kept constant at 1 μM while varying the concentration of added complexes **1**-**3**. The CD results were expressed in terms of the mean residual ellipticity (MRE) in deg cm^2 $dmol^{-1}$ according to the following equ (3)[26]

$$MRE = \frac{Observed\ CD\ (mdeg)}{10C_p nl} \qquad (3)$$

Here, C_p represents the molar concentration of the protein, *n* stands for the number of amino acid residues (583 for BSA) and *l* is the path length of the cell (1 cm). The α-helical (%) contents of the free and bound BSA were calculated from the mean MRE values at 208 nm using the following eqn (4)[27]

$$\alpha - helix\ (\%) = \frac{[-MRE_{208} - 4000]}{[33{,}000 - 4000]} \times 100 \qquad (4)$$

MRE_{208} is the MRE value observed at 208 nm, 4000 is the MRE of the β-form and random coil conformation at 208 nm, and 33000 is the MRE value of a pure α-helix at 208 nm.

7. *Förster Resonance Energy Transfer* (*FRET*)

The value of R_0 was calculated using eqn (5)

$$R_0 = 0.2018 \left[\kappa^2 \phi_D \eta^{-4} J(\lambda)\right] \text{Å} \qquad (5)$$

where the orientation factor between the emission dipole of the donor and the absorption dipole of the acceptor κ^2 is taken as 2/3, the fluorescence quantum yield of the donor ϕ_D is 0.118, the refractive index of the medium (η) is 1.33, and $J(\lambda)$ is the extent of spectral overlap of donor (BSA) emission and the acceptor (complex) absorption spectra.[28] The value of $J(\lambda)$ can be calculated using eqn (6)[29]

$$J(\lambda) = \int_0^\infty \bar{I}_D(\lambda)\varepsilon_A(\lambda)\lambda^4 \, d\lambda \qquad M^{-1}cm^{-1}nm^4 \qquad (6)$$

Where, $\bar{I}_D(\lambda)$ denotes the normalized fluorescence emission of the donor BSA at the wavelength λ, and $\varepsilon_A(\lambda)$ represents the molar extinction coefficient of the acceptor metal complex at the wavelength λ.

Table S1. Summarized crystallographic data and refinement parameters for [Cu(L)(NCS)] (**1**); [Cu(L)(N_3)] (**2**) and [Cu(L)(NO_3)] (**3**)

Crystal parameters	**1**	**2**	**3**
Formula	$C_{25}H_{27}CuN_3OS$	$C_{24}H_{27}CuN_5O$	$C_{24}H_{27}CuN_3O_4$
Formula Weight	481.09	465.04	485.02
Crystal System	*Triclinic*	*Monoclinic*	*Orthorhombic*
Space group	*P-1*	*C2/c*	*Pmcn*
a, b, c [Å]	6.6554(6), 10.5705(8), 17.5161(15)	37.011(3), 6.8204(6), 18.5941(16)	6.999(4), 16.759(10), 19.180(12)

α [°]	86.302(3)	90	90
β [°]	89.149(3)	96.449(3)	90
γ [°]	73.635(3)	90	90
V [Å^3]	1179.88(17)	4664.0(7)	2250(2)
Z	2	8	4
D(calc) [g.cm^{-3}]	1.354	1.325	1.432
μ (Mo-Kα) [mm^{-1}]	1.035	0.961	1.007
F(000)	502	1944	1012
θ(Min-Max) [°]	2.012-27.124	2.215- 26.998	2.124-25.478
Data/restraints/ parameters	5182 / 0 / 280	5052 / 0 / 262	2235/ 0 / 179
R1[a],wR2[b][$I > 2\sigma(I)$]	0.0443; 0.1082	0.0690; 0.1691	0.0708; 0.1923
GOF[c]	1.059	1.021	1.020

[a] $R_1 = \sum |(|F_o| - |F_c|)| / \sum |F_o|$

[b] $wR_2 = [\sum [w (F_o^2 - F_c^2)^2] / \sum [w (F_o^2)^2]]^{1/2}$,

[c] GOF (S) = $\{\sum [w(F_o^2 - F_c^2)^2] / (n - p)\}^{1/2}$, where n = number of measured data and p = number of parameters.

Table S2. Selected X-ray and Calculated (DFT/B3LYP) bond lengths (Å) and angles (°) of **1**, **2** and **3**.

Bonds (Å)	**1**		**2**		**3**	
	X-ray	**Calc.**	**X-ray**	**Calc.**	**X-ray**	**Calc.**
Cu1–O1	1.8694(19)	1.91674	1.887(3)	1.92944	1.871(5)	1.89673
Cu1–N1	1.9483(19)	2.00159	1.963(4)	2.01636	1.952(5)	2.00551
Cu1–N2	1.980(2)	2.06919	1.992(4)	2.07299	2.021(5)	2.03772
Cu1–N3	1.947(2)	1.94619	1.966(5)	1.95007		
Cu1–O2					2.233(5)	2.18895

Cu1–O2					2.233(5)	2.18928
O1–C1	1.302(3)	1.29437	1.290(5)	1.29434	1.324(7)	1.29100
N1–C15	1.300(3)	1.31634	1.290(5)	1.31499		
N1–C16	1.412(3)	1.40655	1.416(5)	1.40369		
N1–C13					1.312(8)	1.31621
N1–C14					1.412(8)	1.40255
N2–C23	1.327(3)	1.32212				
N2–C24	1.371(3)	1.36208				
N2–C21			1.368(6)	1.36218	1.318(9)	1.32296
N2–C22			1.317(6)	1.32155	1.373(8)	1.36518
C1–C2	1.422(4)	1.44454	1.424(6)	1.44982	1.428(9)	1.44685
C1–C6	1.422(3)	1.44435	1.433(6)	1.44511	1.435(9)	1.44323
C6–C15	1.415(3)	1.41440	1.422(6)	1.41591		
C6–C13					1.417(9)	1.41391
Angles (°)						
O1–Cu1–N1	93.27(8)	92.35670	92.28(14)	92.42093	94.4(2)	92.41097
O1–Cu1–N2	174.49(8)	173.16655	171.54(15)	172.93276	177.0(2)	174.18981
O1–Cu1–N3	89.83(9)	95.15211	92.69(19)	97.32927		
N1–Cu1–N2	83.03(9)	80.80984	82.83(16)	80.51184	82.7(2)	81.77884
N1–Cu1–N3	172.64(10)	172.49118	172.39(19)	170.24981		
N2–Cu1–N3	94.33(10)	91.68134	92.9(2)	89.73797		
O1–Cu1–O2					90.82(17)	91.51153
N1–Cu1–O2					151.61(12)	149.97128
N2–Cu1–O2					91.80(19)	93.53153
O2–Cu1–O2					55.9(2)	59.55174

Table S3. Energy and compositions (%) of selected molecular orbitals (**α**-spins) of Complex **1**, **2** and **3**.

MOs	**1**				**2**				**3**			
	E (eV)	% of composition			E (eV)	% of composition			E (eV)	% of composition		
		Cu	NCS	L		Cu	N_3	L		Cu	NO_3	L
LUMO+5	0.54	68	8	24	0.65	59	6	35	0.34	2	0	98
LUMO+4	0.24	12	2	86	0.42	24	3	73	-0.04	0	0	100
LUMO+3	-0.04	1	0	99	0.13	2	0	98	-0.25	10	91	0
LUMO+2	-1.33	0	0	100	-1.16	0	0	100	-1.33	0	0	100
LUMO+1	-1.9	2	0	98	-1.69	2	0	98	-1.88	2	0	98
LUMO	-2.72	0	0	100	-2.53	0	0	99	-2.71	0	0	100
HOMO	-5.31	1	83	16	-5.33	2	21	78	-5.52	2	4	94
HOMO-1	-5.42	2	96	2	-5.67	4	73	22	-6.27	5	72	23
HOMO-2	-5.58	3	15	83	-5.71	11	70	19	-6.5	1	17	82
HOMO-3	-6.46	1	0	99	-6.3	1	1	98	-6.74	14	6	80
HOMO-4	-6.72	13	5	82	-6.72	4	21	72	-7.4	0	33	67
HOMO-5	-7.46	0	0	100	-7.27	0	0	100	-7.45	2	96	2
HOMO-6	-7.81	0	0	100	-7.64	0	0	100	-7.5	1	62	37
HOMO-7	-7.84	15	8	77	-7.77	16	10	74	-7.77	2	92	6
HOMO-8	-8.18	0	1	99	-8.11	0	0	99	-7.83	0	9	90
HOMO-9	-8.39	3	0	97	-8.26	6	0	94	-7.85	11	21	68
HOMO-10	-8.54	3	0	96	-8.46	3	0	97	-8.25	0	0	99

Table S4. Energy and compositions (%) of selected molecular orbitals (**β**-spin) of Complex **1**, **2** and **3**.

MOs	**1**		**2**		**3**	
	E (eV)	% of composition	E (eV)	% of composition	E (eV)	% of composition

		Cu	NCS	L		Cu	N_3	L		Cu	NO_3	L
LUMO+5	0.24	14	2	84	0.42	26	3	71	-0.02	0	0	100
LUMO+4	-0.03	1	0	99	0.14	2	0	98	-0.24	10	91	0
LUMO+3	-1.33	0	0	100	-1.16	0	0	100	-1.33	0	0	100
LUMO+2	-1.87	2	0	98	-1.66	2	0	98	-1.85	2	0	98
LUMO+1	-2.71	0	0	99	-2.52	0	0	99	-2.71	0	0	100
LUMO	-3.1	56	13	31	-2.74	52	23	26	-3.13	61	5	34
HOMO	-5.26	1	82	17	-5.26	2	30	68	-5.46	2	6	92
HOMO-1	-5.39	4	91	4	-5.58	5	64	31	-6.16	7	76	16
HOMO-2	-5.55	3	16	81	-5.93	10	73	16	-6.47	1	10	89
HOMO-3	-6.45	1	0	99	-6.29	1	1	98	-7.2	8	5	86
HOMO-4	-7.16	9	2	98	-7.07	12	4	84	-7.38	0	48	52
HOMO-5	-7.45	1	0	99	-7.26	1	0	99	-7.45	2	94	4
HOMO-6	-7.81	0	0	100	-7.64	0	0	100	-7.47	2	47	52
HOMO-7	-8.17	0	1	99	-8.11	0	0	99	-7.73	3	94	3
HOMO-8	-8.34	7	1	92	-8.19	13	0	87	-7.83	0	6	94
HOMO-9	-8.51	4	1	96	-8.43	4	0	96	-8.24	0	1	99
HOMO-10	-8.63	5	2	94	-8.52	44	1	56	-8.36	7	1	92

Table S5. Vertical electronic transitions of Complexes **1**, **2** and **3** calculated by TDDFT/B3LYP/CPCM method in DMSO medium.

Compds.	λ (nm)	E (eV)	Osc. Strength (f)	Key excitations	Character[a]	$\lambda_{expt.}$ (nm) (ε ($M^{-1}cm^{-1}$))
	584	2.1213	0.0175	(57%)HOMO-2→LUMO(β)	L(π)→Cu(dπ)	

					LMCT	
	466	2.6605	0.1334	(31%)HOMO→LUMO(α) (30%)HOMO→LUMO+1(β)	$NCS^-/L(\pi)\rightarrow L(\pi^*)$ ILCT	**470** **(1.64×10^4)**
1	367	3.3768	0.1628	(34%)HOMO-1→LUMO(α) (55%)HOMO-1→LUMO+1(β)	$NCS^-\rightarrow L(\pi^*)$ ILCT	**362** **(1.75×10^4)**
	358	3.4656	0.1251	(60%)HOMO-3→LUMO(α) (33%)HOMO-2→LUMO+1(β)	$L(\pi)\rightarrow L(\pi^*)$ ILCT	**344** **(2.38×10^4)**
	340	3.6431	0.3442	(56%)HOMO-5→LUMO(β)	$L(\pi)\rightarrow Cu(d\pi)$ LMCT	
	529	2.3437	0.0432	(56%)HOMO-3→LUMO(β)	$N_3^-\rightarrow Cu(d\pi)$ LMCT	
	469	2.6452	0.2054	(45%)HOMO→LUMO(α) (44%)HOMO→LUMO+1(β)	$L(\pi)/N_3^-\rightarrow L(\pi^*)$ ILCT	**471** **(1.69×10^4)**
2	357	3.4702	0.3571	(45%)HOMO-3→LUMO(α) (43%)HOMO-2→LUMO+1(β)	$L(\pi)/N_3^-\rightarrow L(\pi^*)$ ILCT	**345** **(2.55×10^4)**
	329	3.7687	0.2456	(23%)HOMO→LUMO+1(α) (46%)HOMO-5→LUMO(β)	$L(\pi)\rightarrow L(\pi^*)$, ILCT $L(\pi)\rightarrow Cu(d\pi)$, LMCT	**330** **(2.52×10^4)**
	299	4.1499	0.1630	(50%)HOMO-3→LUMO+1(α) (36%)HOMO-2→LUMO+2(β)	$L(\pi)/N_3^-\rightarrow L(\pi^*)$ ILCT	
	473	2.6217	0.1963	(47%)HOMO→LUMO(α) (44%)HOMO→LUMO+1(β)	$L(\pi)\rightarrow L(\pi^*)$ ILCT	**470** **(2.21×10^4)**
	365	3.3979	0.1726	(43.18%)HOMO-1→LUMO (α) (42.24%)HOMO-1→LUMO+1(β)	$NO_3^-\rightarrow L(\pi^*)$ ILCT	**363** **(2.59×10^4)**
3	348	3.5671	0.4797	(25%)HOMO→LUMO+1(α) (37%)HOMO-4→LUMO(β)	$L(\pi)\rightarrow L(\pi^*)$, ILCT $L(\pi)\rightarrow Cu(d\pi)$, LMCT	**346** **(3.31×10^4)**
	303	4.0970	0.1333	(35%)HOMO-3→LUMO(α) (27%)HOMO-1→LUMO+2 (β)	$L(\pi)/NO_3^-\rightarrow L(\pi^*)$ ILCT	**290** **(0.248×10^5)**

[a] ILCT: Intra-ligand charge transfer; LMCT: Ligand to metal charge transfer.

Table S6. Contour plots of some selected molecular orbitals of Complexes **1**, **2** and **3** calculated by **DFT/B3LYP** method in gas phase (basis set: LanL2DZ) (**α**-spins)

MOs	1	2	3

LUMO +2	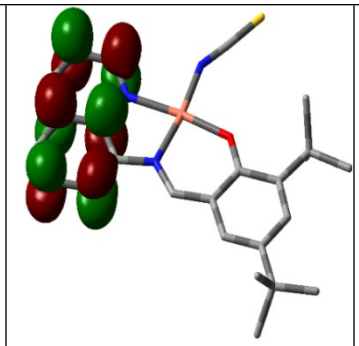	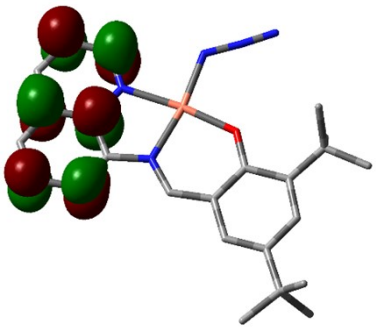	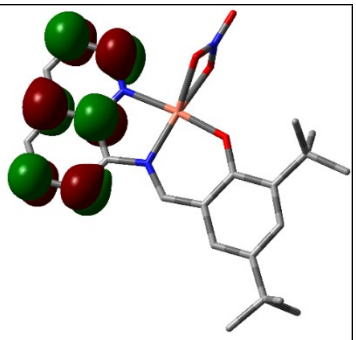
LUMO +1	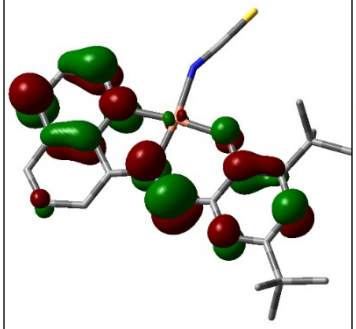	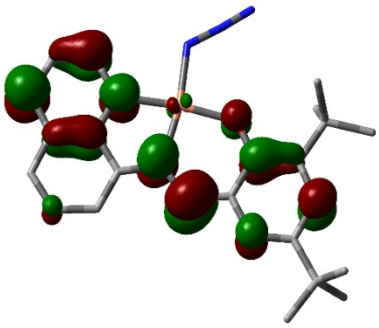	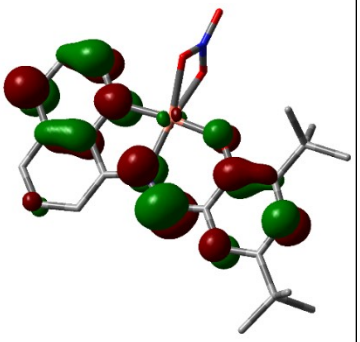
LUMO	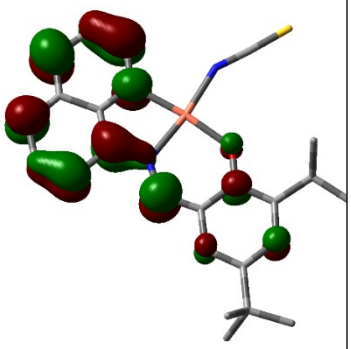	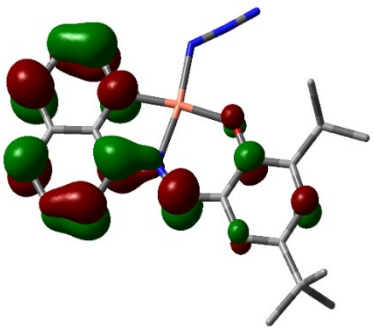	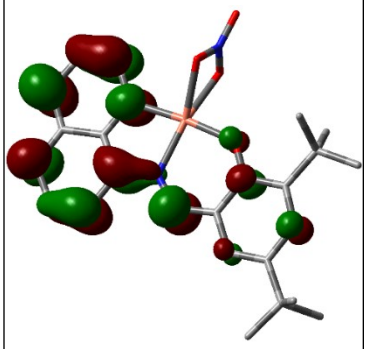
HOMO	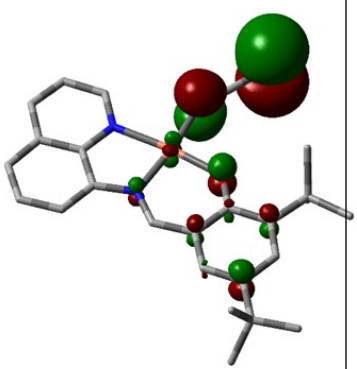	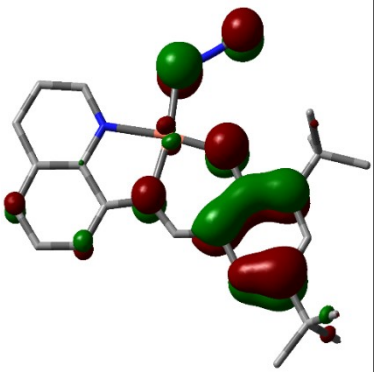	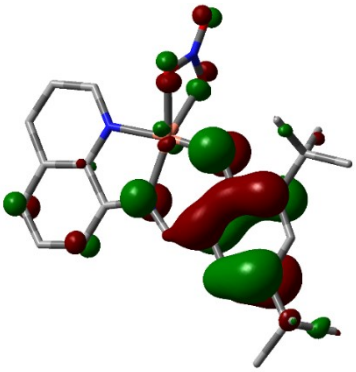

HOMO -1	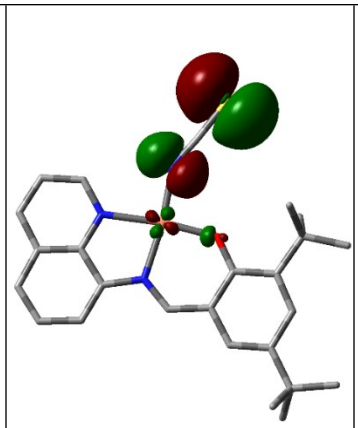	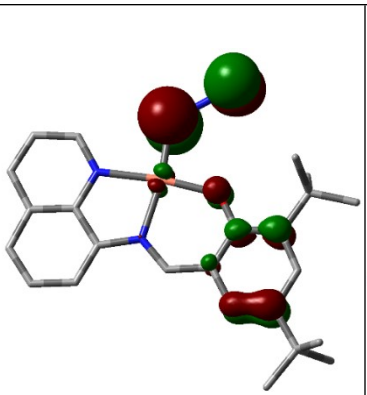	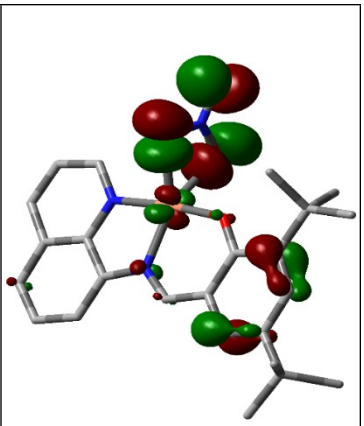
HOMO -2	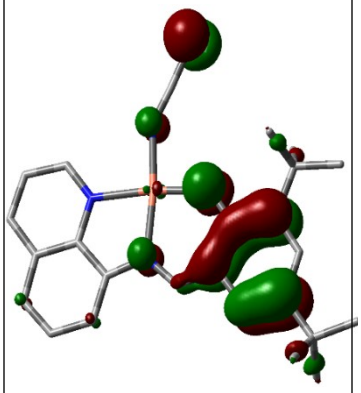	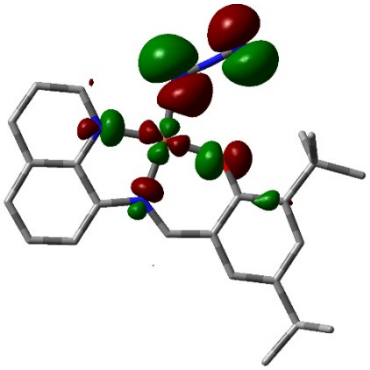	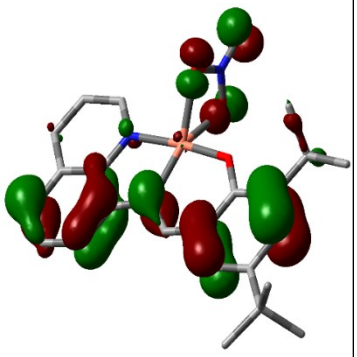

Table S7. Contour plots of some selected molecular orbitals of Complexes **1**, **2** and **3** calculated by **DFT/B3LYP** method in gas phase (basis set: LanL2DZ) (**β**-spin)

MOs	1	2	3

LUMO +2	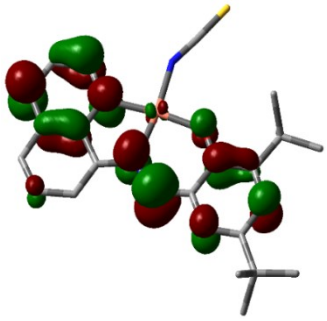	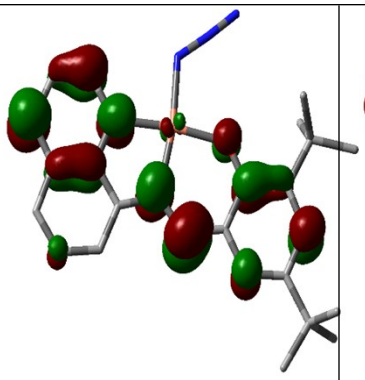	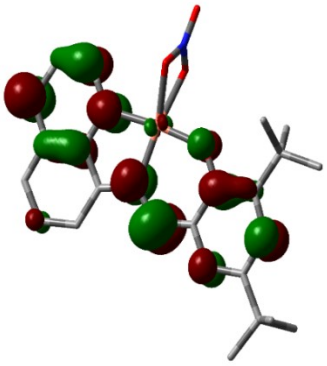
LUMO +1	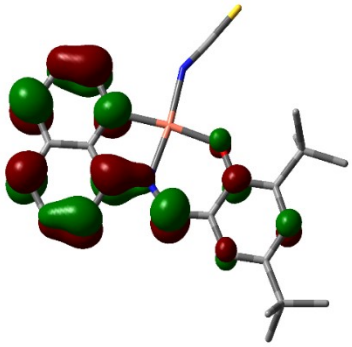	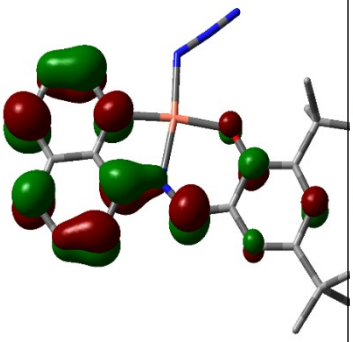	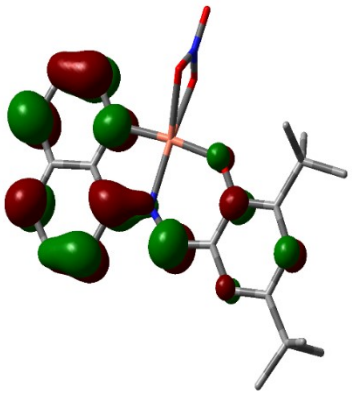
LUMO	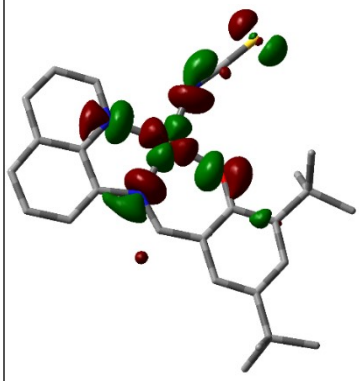	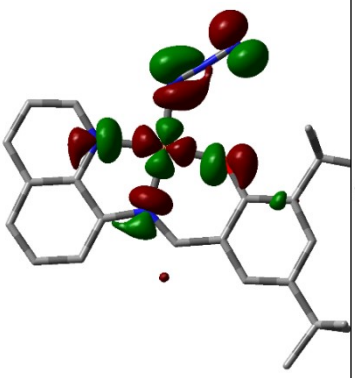	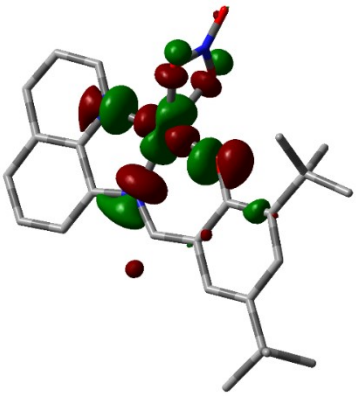
HOMO	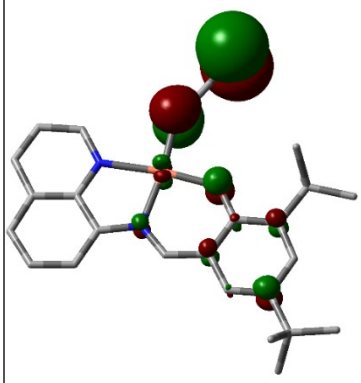	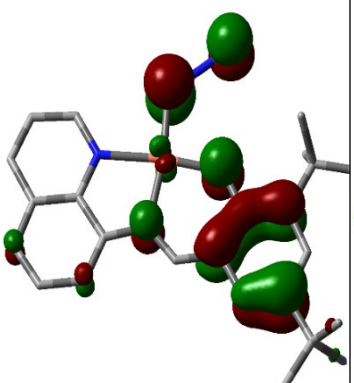	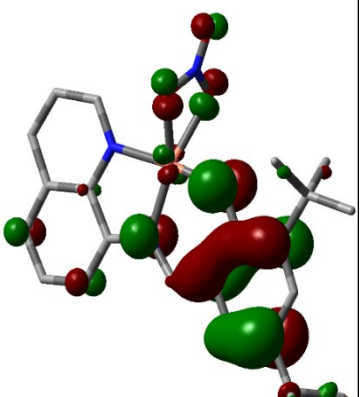

HOMO -1	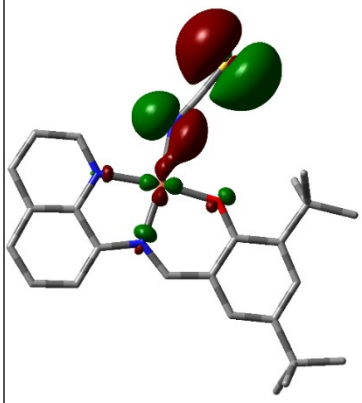	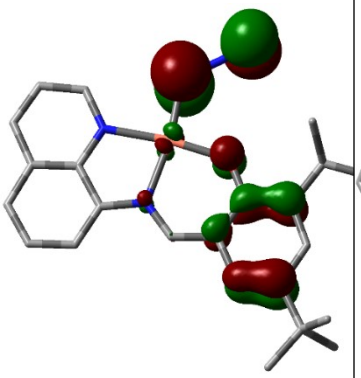	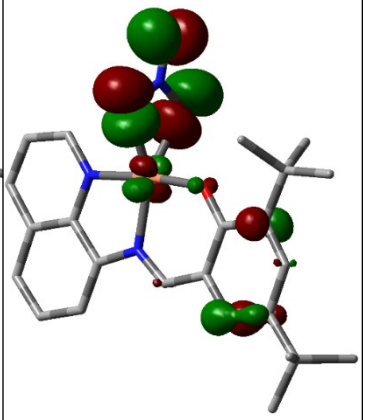
HOMO -2	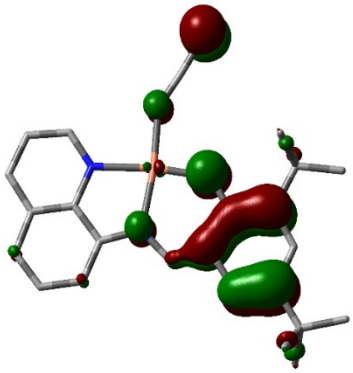	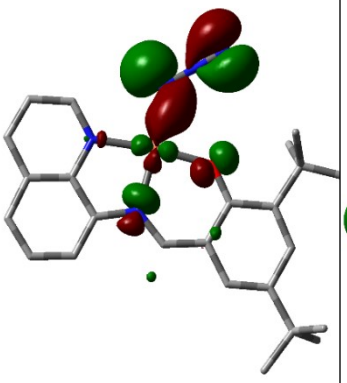	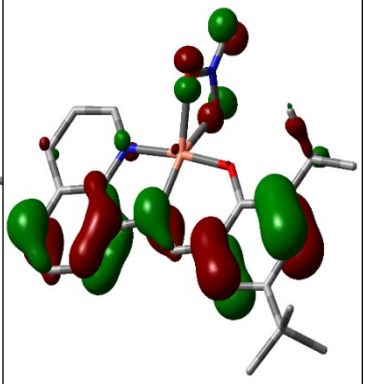

Table S8. Kinetic parameters of catecholase activity at 298K for complex **1**, **2** and **3**.

Complex	V_{max} (M min^{-1})	K_M (M)	K_{cat} (h^{-1})	Ref
1	**4.11×10^{-5}**	**2.87×10^{-3}**	**49.3**	**This work**

2	**4.33×10^{-5}**	**2.99×10^{-3}**	**52.0**	**This work**
3	**5.76×10^{-5}**	**4.49×10^{-3}**	**69.1**	**This work**
$[Cu_2(L^1)_2(mb)]\cdot ClO_4$ (1)	**2.31×10^{-7}**	**1.90×10^{-3}**	**42.0**	**30a**
$[Cu_2(L^2)_2(mb)]\cdot ClO_4$ (2)	**2.91×10^{-7}**	**2.76×10^{-3}**	**52.9**	
$[Cu_2(L^4)(OMe)(MeOH)(ClO_4)]ClO_4$		**3.1×10^{-4}**	**48.0**	**30b**
$[Cu(L^{11})(phen)][Cu(L^{11})(phen)].5H_2O$	**3.4×10^{-5}**	**2.4×10^{-3}**	**62**	**30c**
$[Cu(L^{12})(phen)](ClO_4)$	**2.8×10^{-5}**	**2.3×10^{-3}**	**52**	**30c**
$[Cu_2(H_2LDA)(ClO_4)](ClO_4)$		**3.5×10^{-3}**	**58.68**	**30d**
$[Cu(L)(phen)](ClO_4)$	**6.103×10^{-7}**	**2.945×10^{-3}**	**73.574**	**30e**

Table S9. Kinetic parameters of Phenoxazinone synthase like-activities at 298K for complex **1**, **2** and **3**.

Complex	V_{max} (M min^{-1})	K_M (M)	K_{cat} (h^{-1})	Ref
1	**1.18×10^{-7}**	**2.97×10^{-3}**	**1.42×10^{-1}**	**This work**
2	**1.26×10^{-7}**	**2.96×10^{-3}**	**1.51×10^{-1}**	**This work**
3	**1.52×10^{-7}**	**1.95×10^{-3}**	**1.82×10^{-1}**	**This work**
Complex 1	**2.07×10^{-6}**	**2.32×10^{-3}**	**2.5**	**19c**
Complex 2	**2.02×10^{-6}**	**2.80×10^{-3}**	**2.4**	
Complex 3	**1.83×10^{-6}**	**2.46×10^{-3}**	**2.2**	
$[(CH_3CN)Cu(L)_2Cu](ClO_4)_2$	**1.11×10^{-3}**	**1.70×10^{-2}**	**11.1**	**31**
$[Cu(L^1)(Cl)_2]$. MeOH	**2.61×10^{-6}**	**14.60×10^{-5}**	**6.264**	**19d**
$[Cu(L^2)(Cl)_2]$. H_2O	**3.19×10^{-6}-**	**13.21×10^{-5}**	**7.668**	
$[Cu(L^3)(Cl)_2]$	**3.51×10^{-6}**	**5.33×10^{-5}**	**8.424**	

Table S10. DNA binding parameters of complexes **1**–**3** and ligand **LH**.

Complex	UV Titration			EB exchange		
	λ_{max} (nm)	Hypo. (%)	K_b (M^{-1})	λ_{max} (nm)	Hypo. (%)	K_{sv} (M^{-1})
1	470	16.99	$(5.70 \pm 0.24) \times 10^4$	608	36.17	$(3.35 \pm 0.12) \times 10^4$
2	471	24.24	$(7.08 \pm 0.29) \times 10^4$	608	39.60	$(3.98 \pm 0.02) \times 10^4$
3	470	30.23	$(2.35 \pm 0.03) \times 10^5$	608	44.6	$(1.72 \pm 0.04) \times 10^5$
LH	345	10.26	$(1.25 \pm 0.05) \times 10^4$	610	18.41	$(1.99 \pm 0.07) \times 10^4$

Table S11. Variation of lifetimes (τ) of BSA (1μM) with increasing concentrations of complex **1**, **2** and **3**.

Environment	**τ_1 (ns)**	**α_1**	**τ_2 (ns)**	**α_2**	**<τ> (ns)**	**χ^2**
BSA	1.637975	14.43	6.05704	85.57	**5.42**	0.9890031
BSA+ [**1**] (1:5)	1.73882	16.09	6.095576	83.91	5.39	0.989368
BSA+ [**1**] (1:10)	1.570463	16.87	6.027365	83.13	5.28	1.07283
BSA+ [**2**] (1:5)	1.544292	16.47	6.047776	83.53	5.31	1.081406
BSA+ [**2**] (1:10)	1.453359	16.55	6.043539	83.45	5.28	1.030847
BSA+ [**3**] (1:5)	1.567623	16.22	6.062117	83.78	5.33	1.047923
BSA+ [**3**] (1:10)	1.732827	18.72	6.119877	81.28	5.29	1.020772

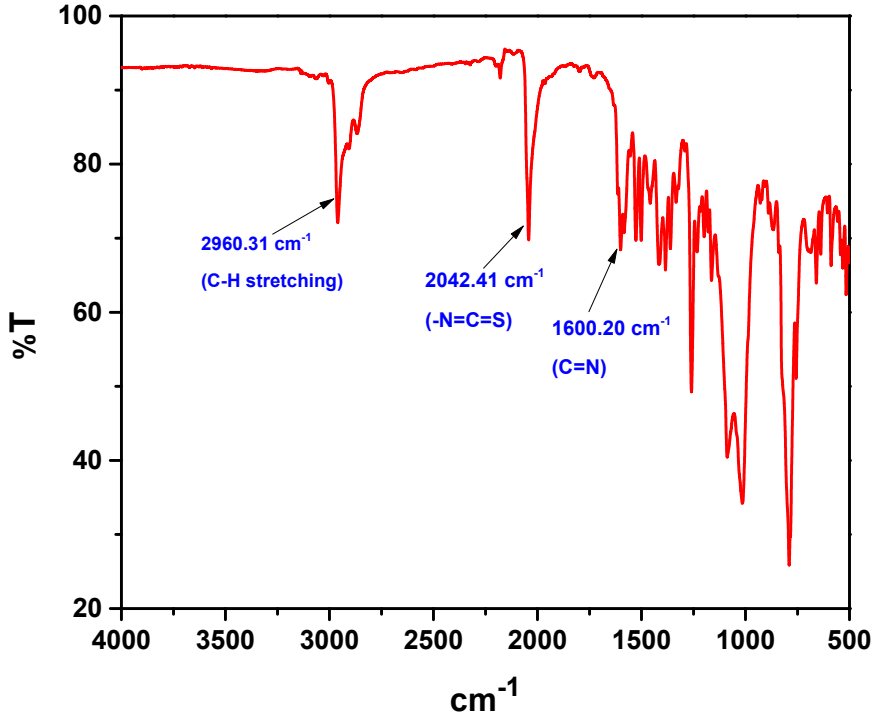
100
80
60
40
20
%T
4000
3500
3000
2500
2000
1500
1000
500
cm-1
2960.31 cm-1
(C-H stretching)
2042.41 cm-1
(-N=C=S)
1600.20 cm-1
(C=N)

[Cu(L)(NCS)] (1)

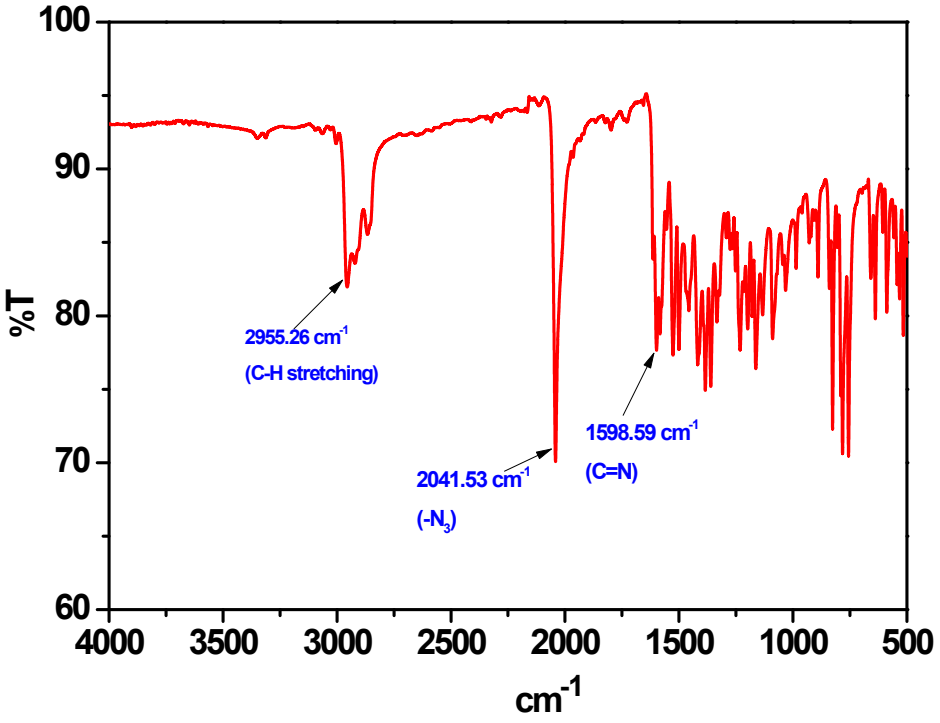
100
90
80
70
60
%T
4000
3500
3000
2500
2000
1500
1000
500
cm-1
2955.26 cm-1
(C-H stretching)
2041.53 cm-1
(-N3)
1598.59 cm-1
(C=N)

[Cu(L)(N_3)] (2)

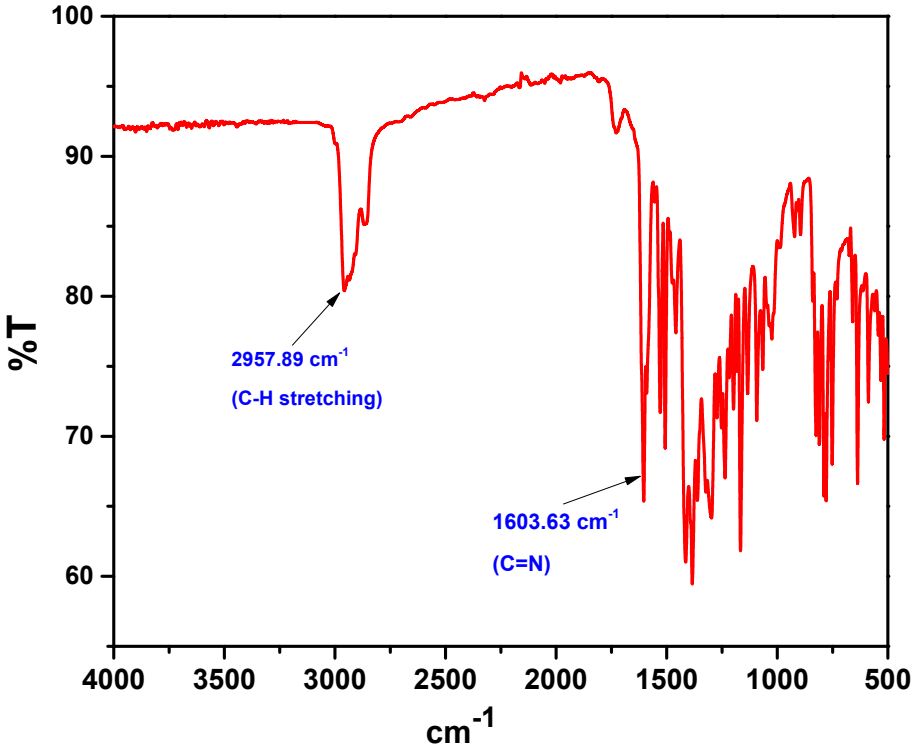
100
90
80
70
60
%T
4000
3500
3000
2500
2000
1500
1000
500
cm-1
2957.89 cm-1
(C-H stretching)
1603.63 cm-1
(C=N)

[Cu(L)(NO_3)] (3)

Figure S1: FT-IR spectra of the complex **1, 2 and 3.**

Figure S2: ESI-Mass spectra of the complex **1, 2 and 3**

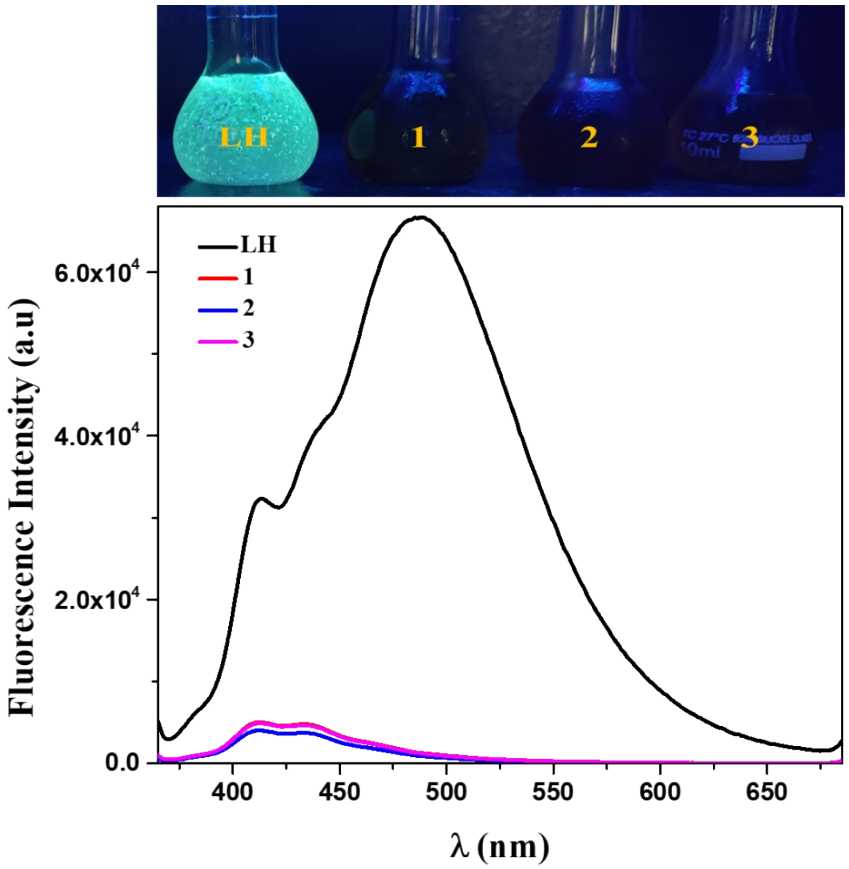

Figure S3: Fluorescence spectra of the Ligand (**LH**) and complex **1, 2 and 3** in DMSO when excited at 350 nm

	d_{norm}	Shape index	Curvedness
1	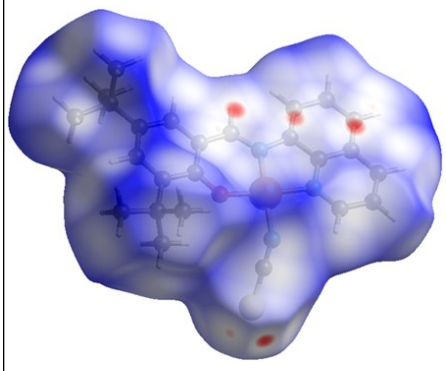	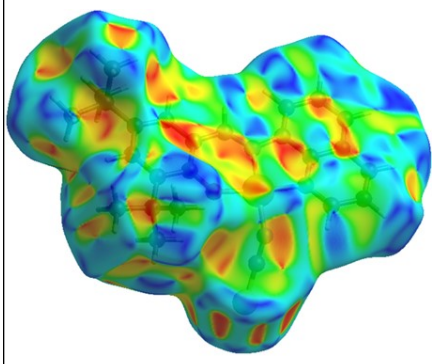	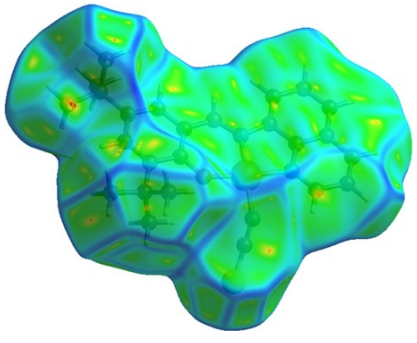
	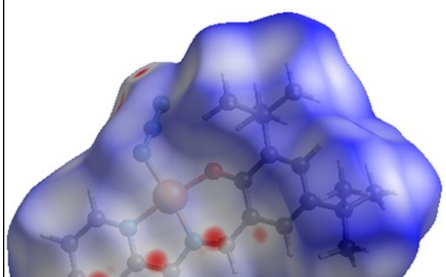	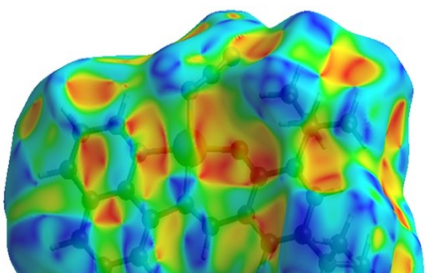	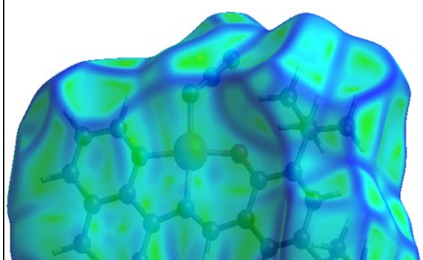

2			
3	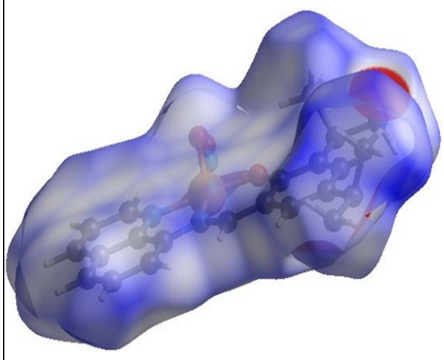	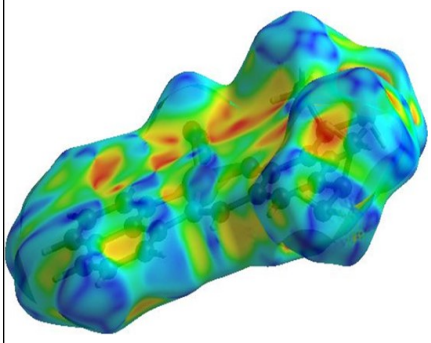	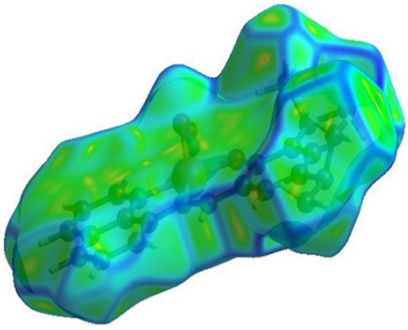

Figure S4: Hirshfeld surfaces mapped with d_{norm} (left-side), shape index (middle) and curvedness (right-side).

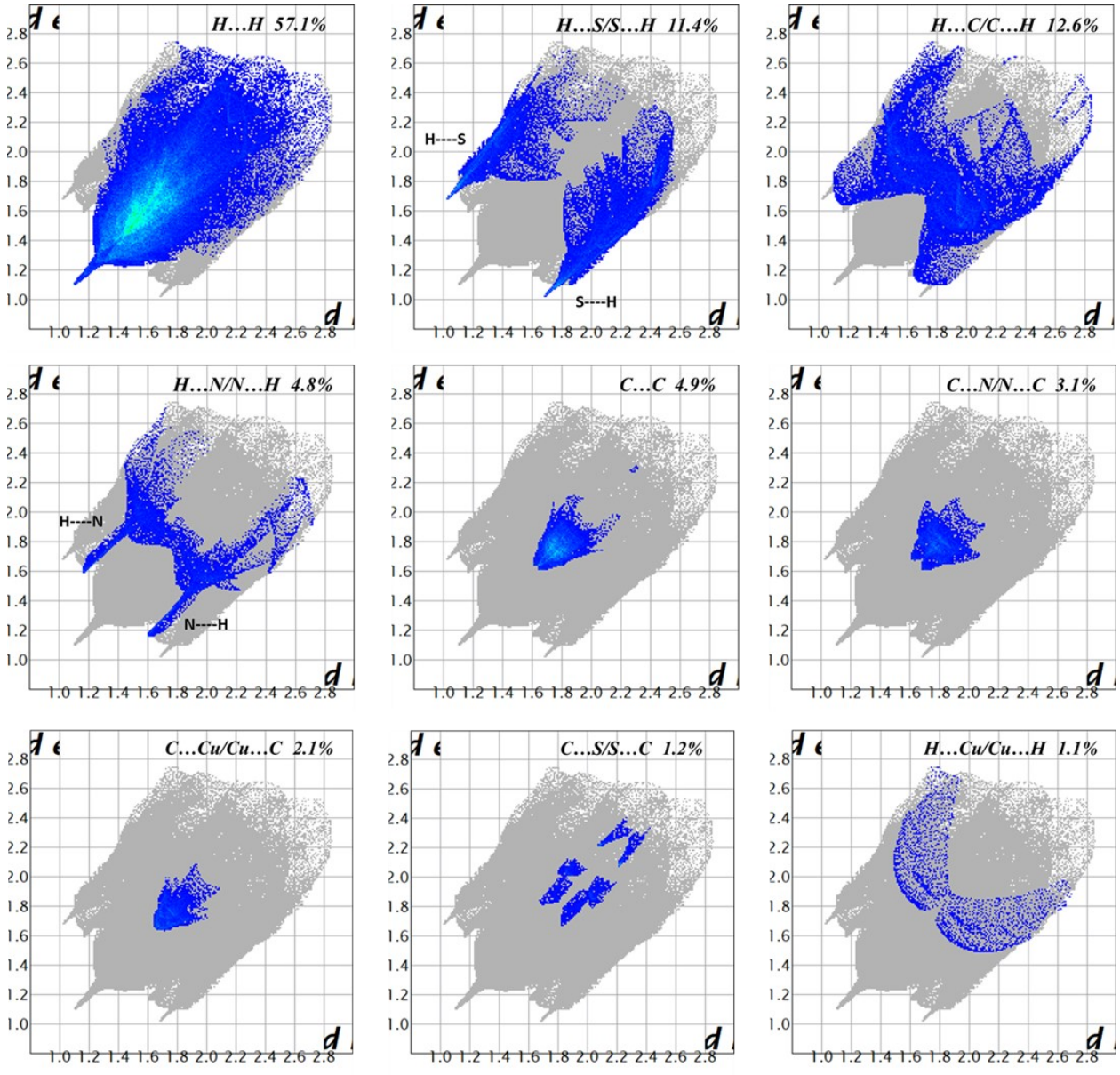

Figure S5: 2D Fingerprint plot resolved into different contacts contributed to the total Hirshfeld Surface area of the complex **1**

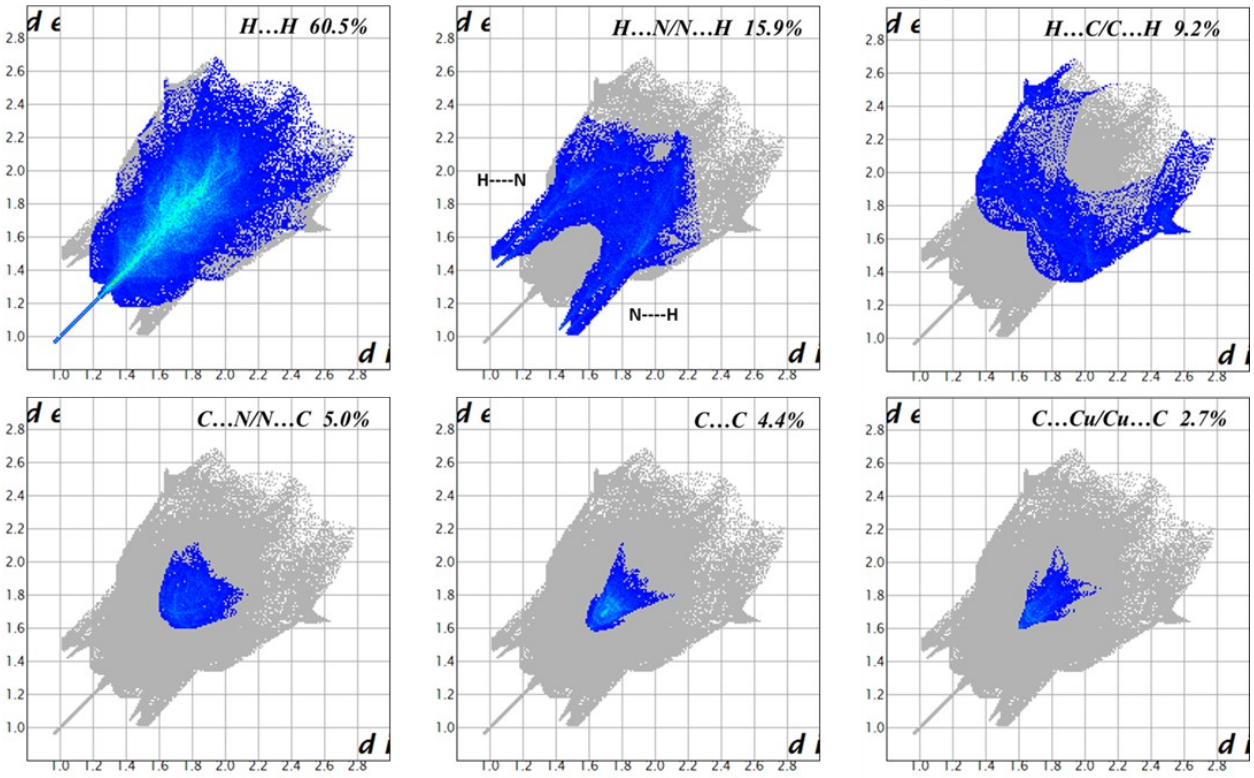

Figure S6: 2D Fingerprint plot resolved into different contacts contributed to the total Hirshfeld Surface area of the complex **2.**

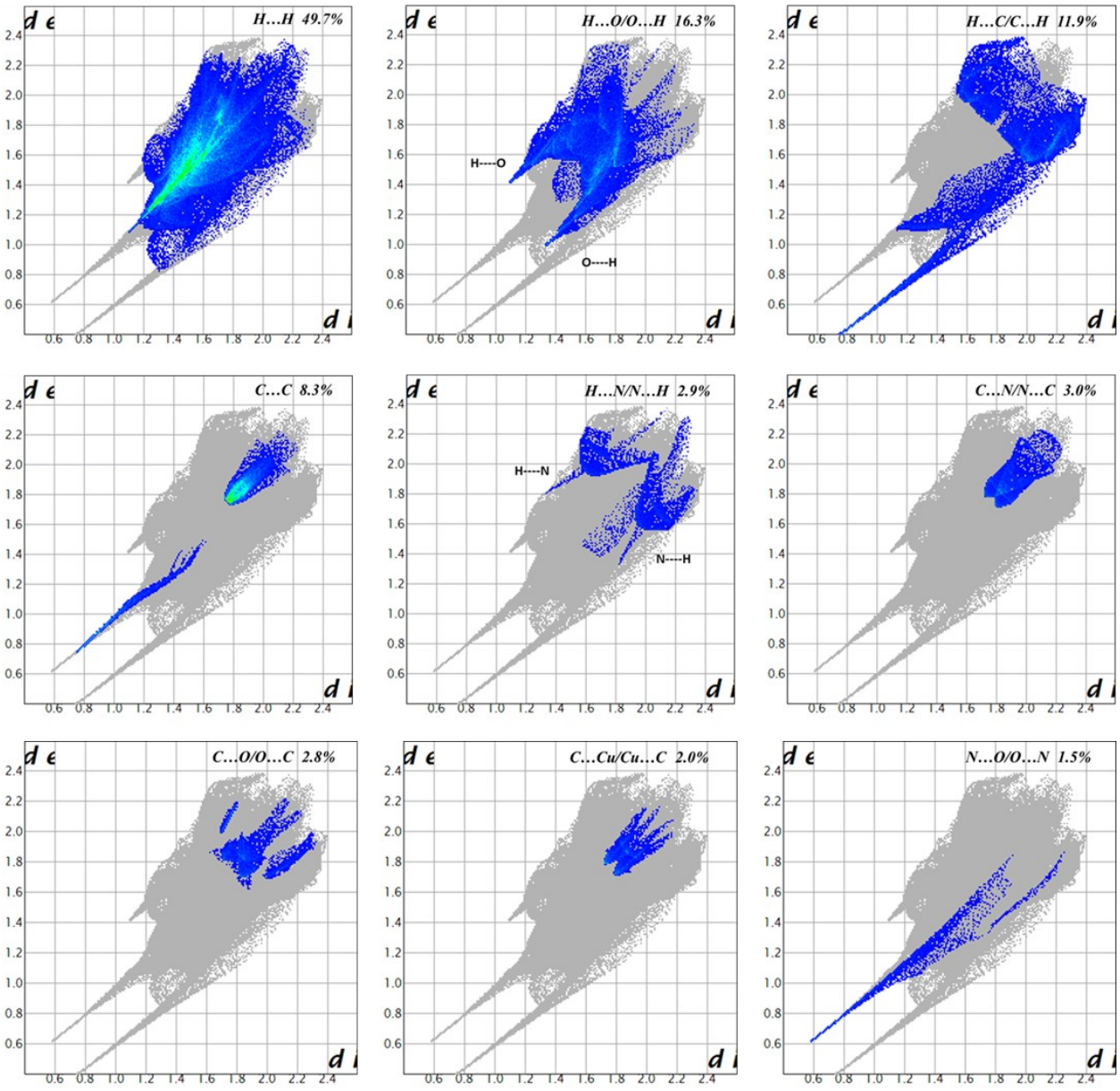

Figure S7: 2D Fingerprint plot resolved into different contacts contributed to the total Hirshfeld Surface area of the complex **3.**

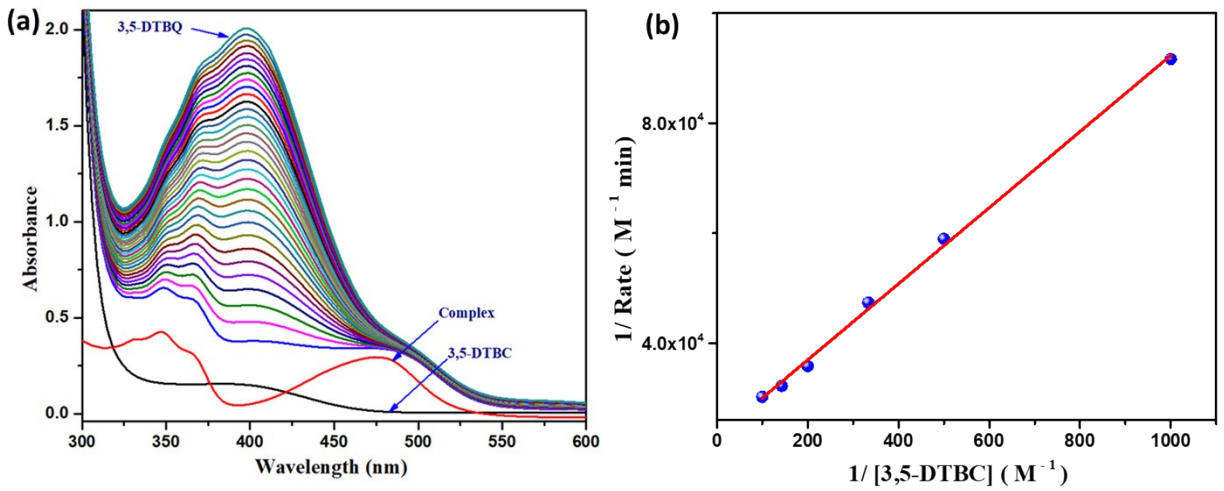

Figure S8: (a) Time dependent UV–Vis spectral growth of 3, 5-DTBQ at ~400 nm upon addition of 1.0×10^{-2} M substrate to 1.0×10^{-4} M of complex-**2** in acetonitrile medium at room temperature. (b) Dependence of rate of catechol oxidation on 3,5-DTBC concentration : Lineweaver–Burk plot

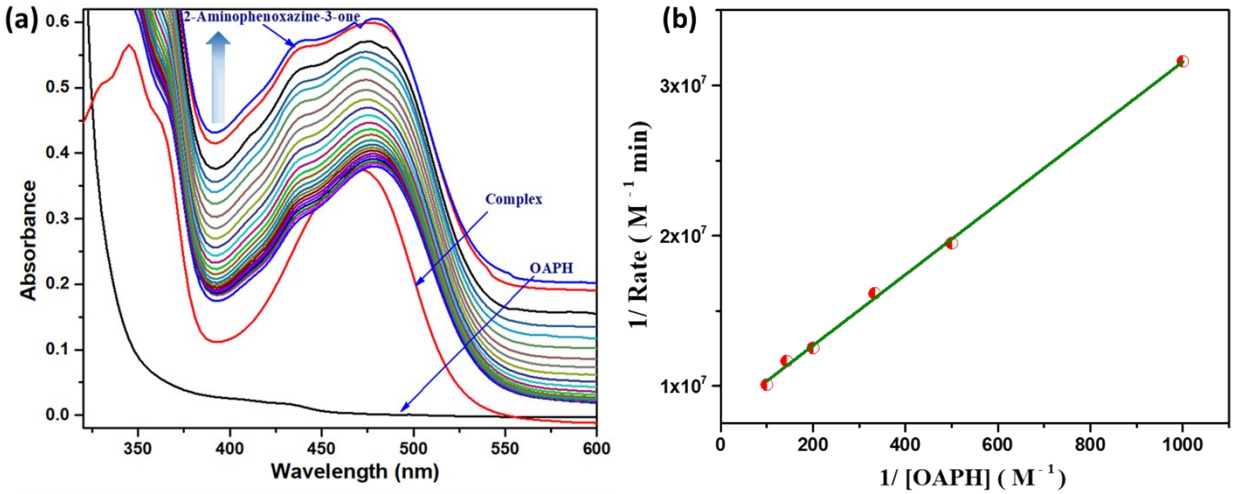

Figure S9: (a) Time dependent UV–Vis spectral growth of APX at ~436 nm upon addition of 1.0×10^{-2} M substrate to 1.0×10^{-4} M of complex-**2** in acetonitrile medium at room temperature. (b) Dependence of rate of oxidation on OAPH concentration : Lineweaver–Burk plot

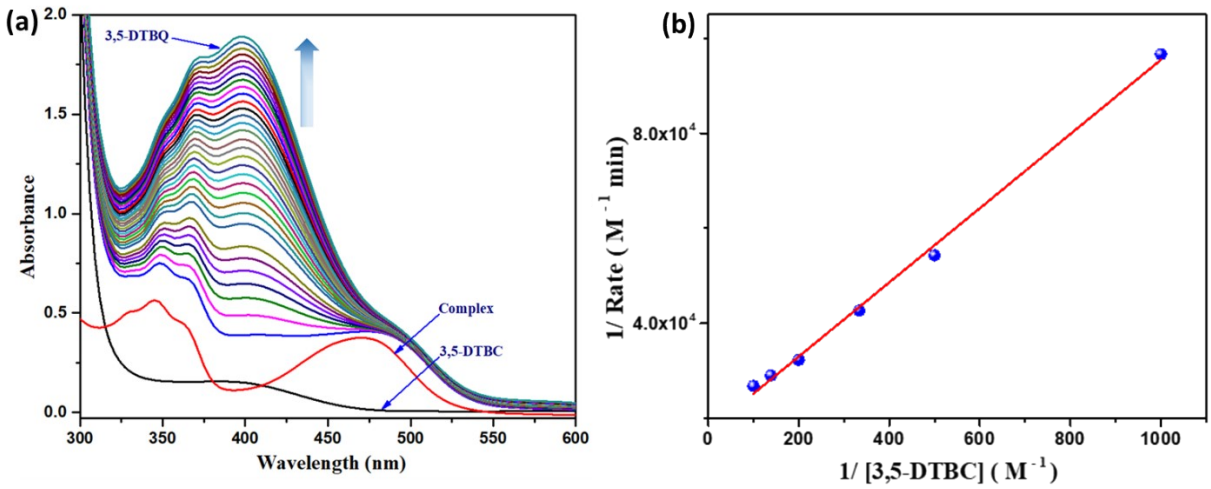

Figure S10: (a) Time dependent UV–Vis spectral growth of 3, 5-DTBQ at ~400 nm upon addition of 1.0×10^{-2} M substrate to 1.0×10^{-4} M of complex-**3** in acetonitrile medium at room temperature. (b) Dependence of rate of catechol oxidation on 3,5-DTBC concentration : Lineweaver–Burk plot

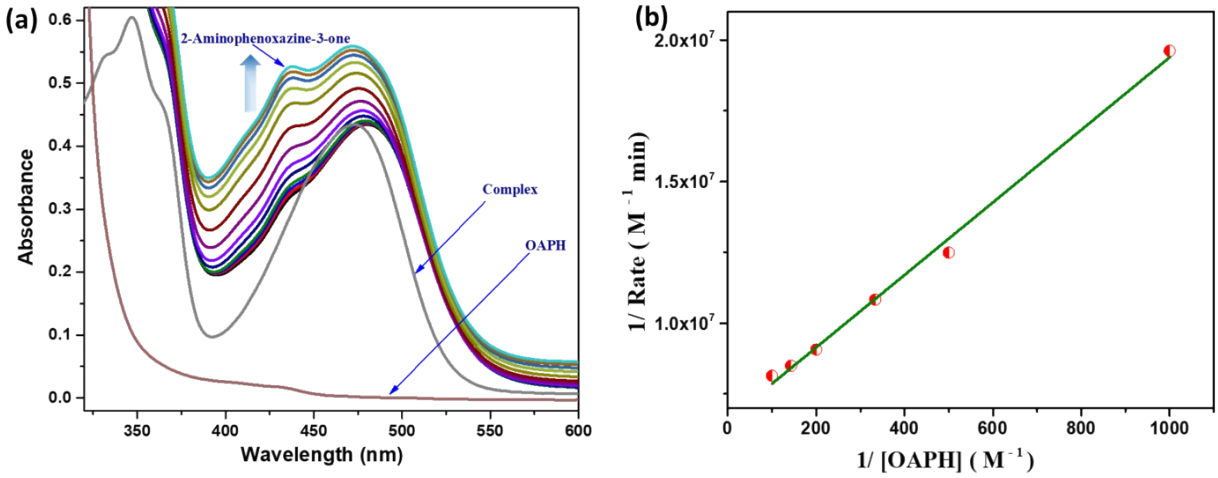

Figure S11: (a) Time dependent UV–Vis spectral growth of APX at ~436 nm upon addition of 1.0×10^{-2} M substrate to 1.0×10^{-4} M of complex-**3** in acetonitrile medium at room temperature. (b) Dependence of rate of oxidation on OAPH concentration : Lineweaver–Burk plot.

Control Experiments	**Using Ligand (LH)**	**Using $Cu(ClO_4)_2.6H_2O$**
Catecholase activity	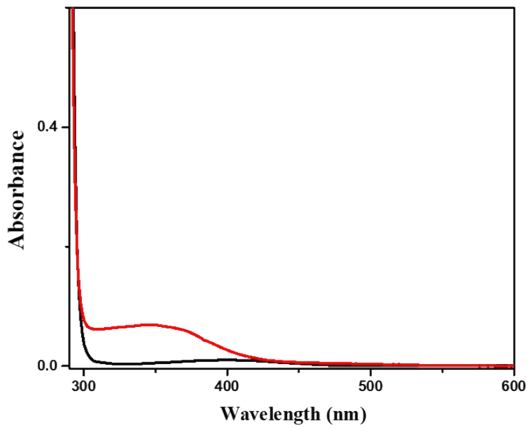	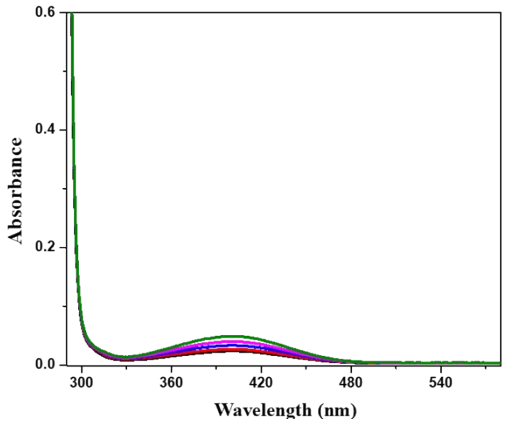
Phenoxazinone synthase like activity	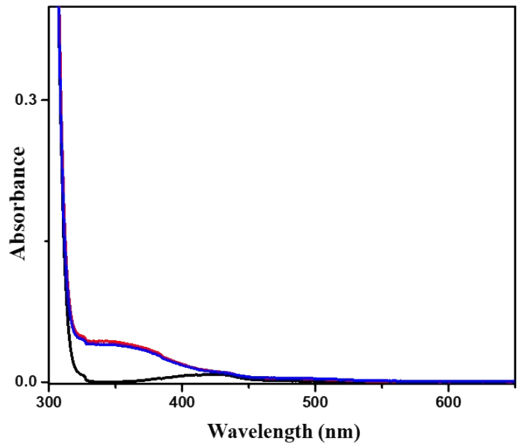	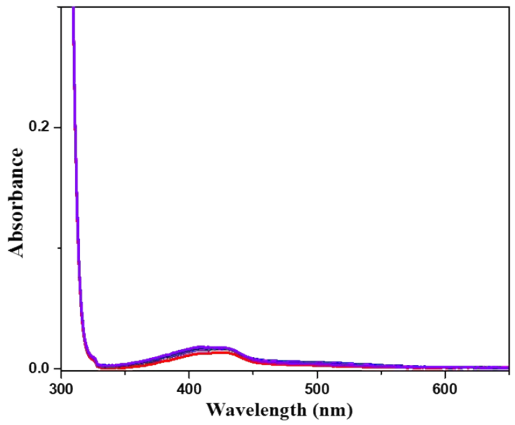

Figure S12: Control Experiments Using Ligand (**LH**) and $Cu(ClO_4)_2.6H_2O$ salt for Catechol oxidase and Phenoxazinone synthase mimicking activity.

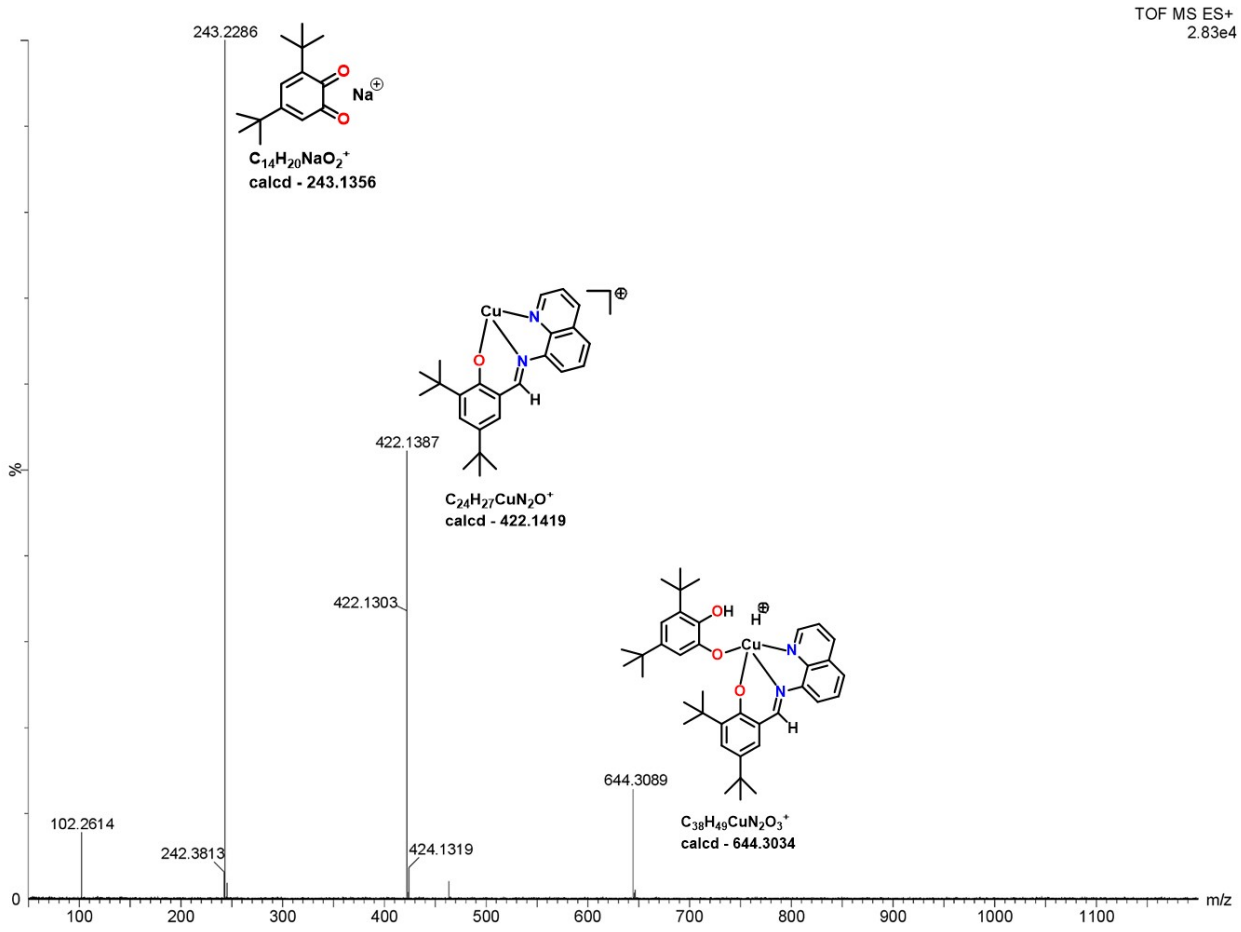

Figure S13: Electrospray ionization mass spectra of 1:50 mixture of the complex **1** and 3,5-DTBC in acetonitrile.

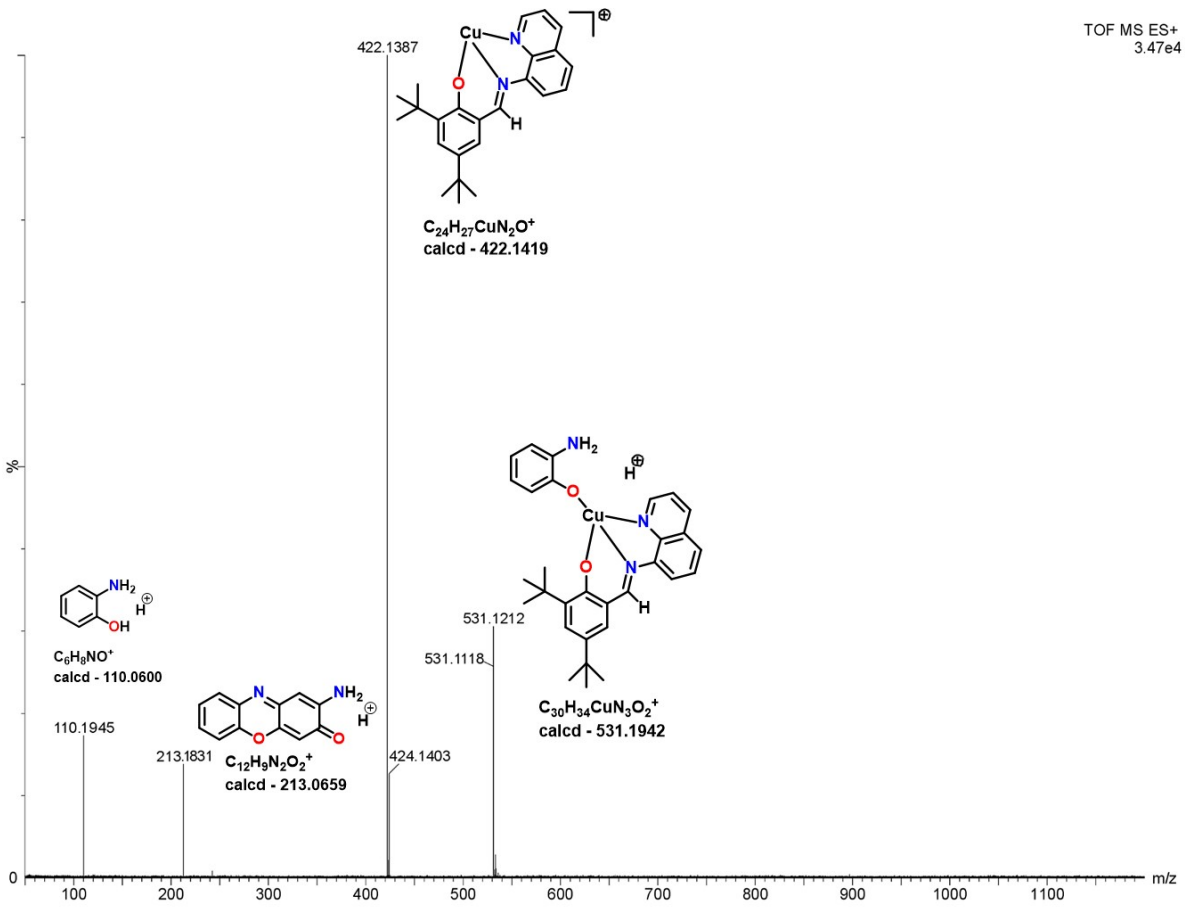

Figure S14: Electrospray ionization mass spectra of 1:50 mixture of the complex **1** and OAPH in acetonitrile.

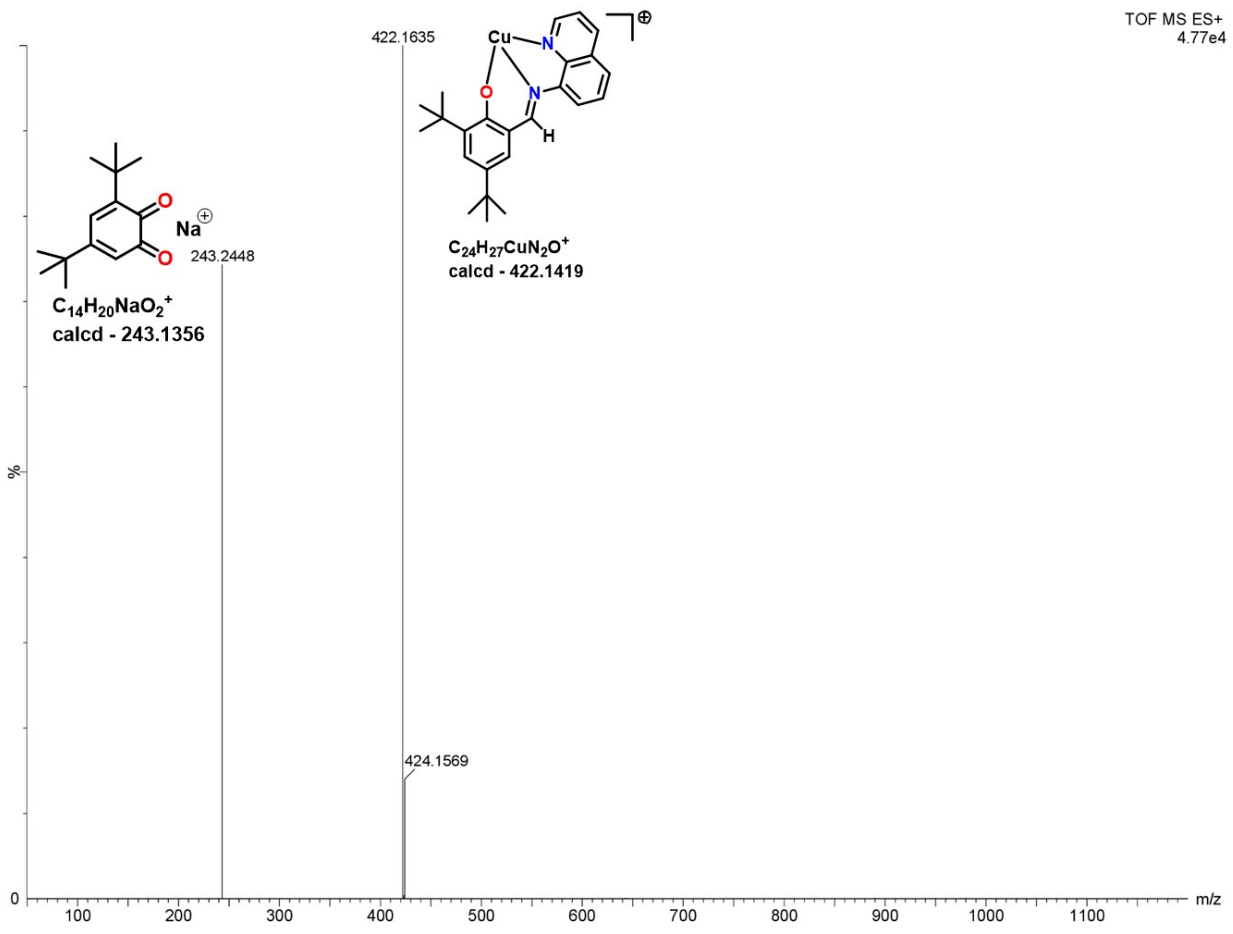

Figure S15: Electrospray ionization mass spectra of 1:50 mixture of the complex **1** and 3,5-DTBC, after 24 hours.

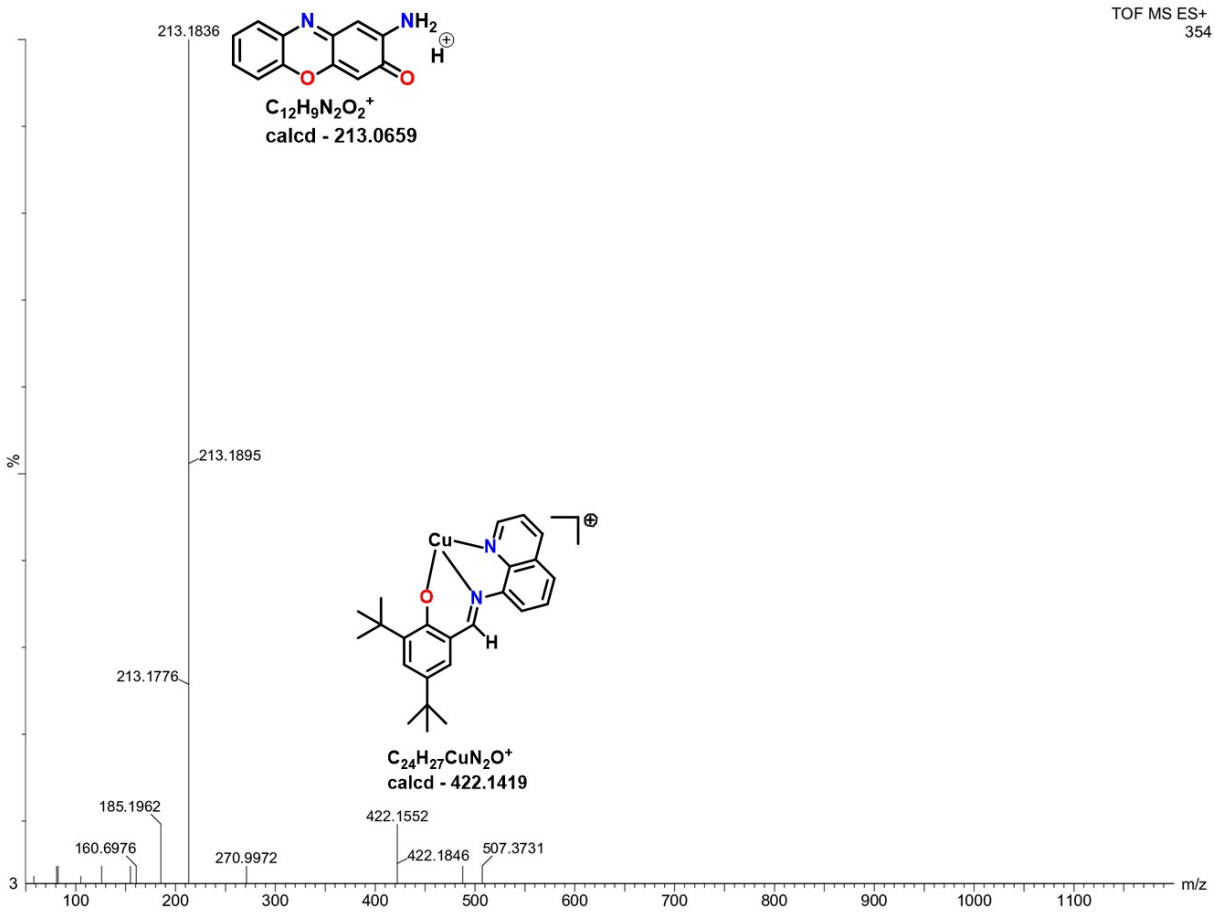

Figure S16: Electrospray ionization mass spectra of 1:50 mixture of the complex **1** and OAPH, after 24 hours.

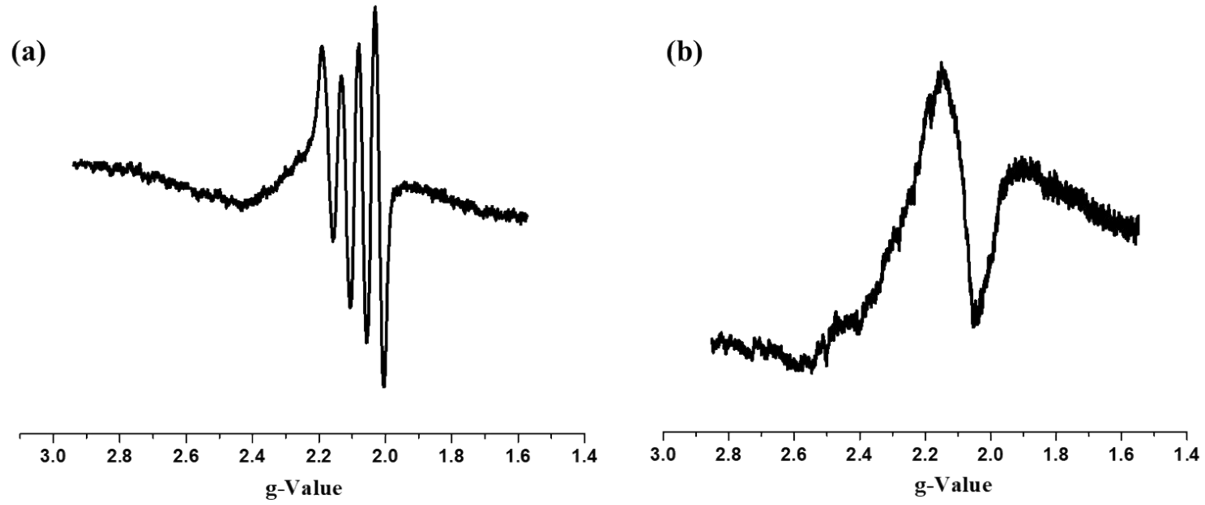

Figure S17: X-band EPR spectra of copper(II) complex **1** in acetonitrile medium, recorded at (a) 298 K, (b) 133 K.

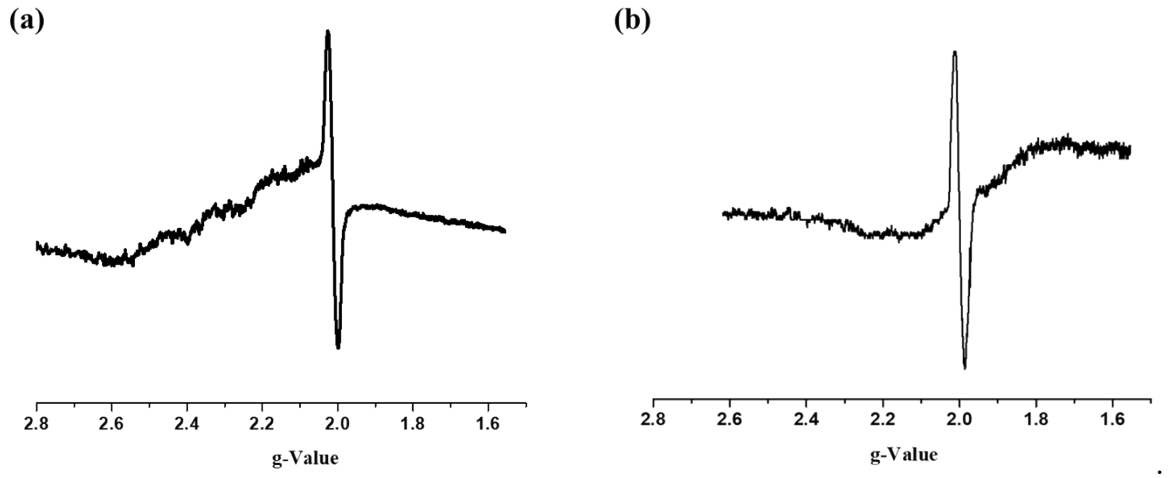

Figure S18: X-band EPR spectra of complex **1** with 3,5-DTBC in acetonitrile medium, recorded at (a) 298 K, (b) 133 K.

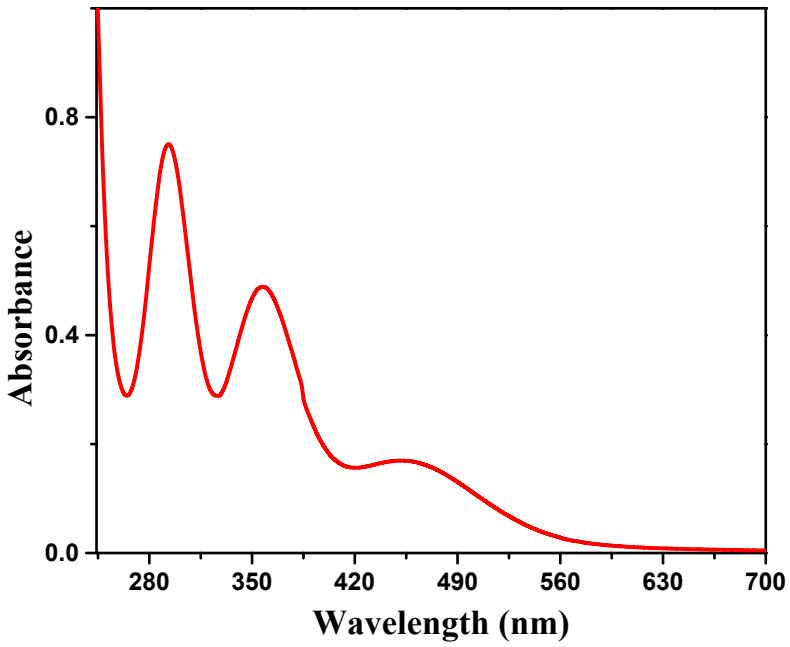

Figure S19: Absorbance profile of I_3^-

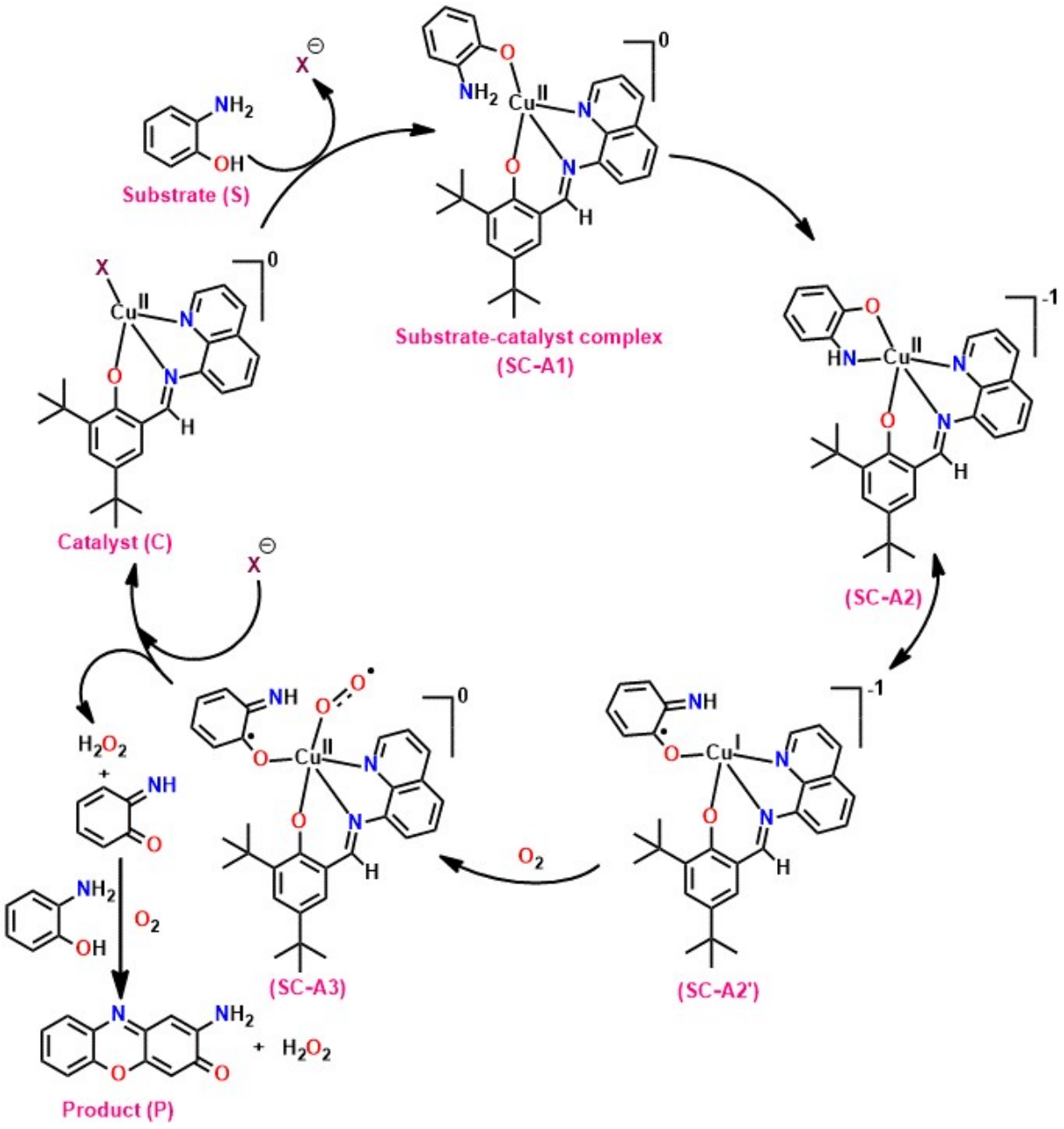

Figure S20: Proposed mechanistic pathway for the aerial oxidation of o-aminophenol to phenoxazinone in presence of the complex **1**.

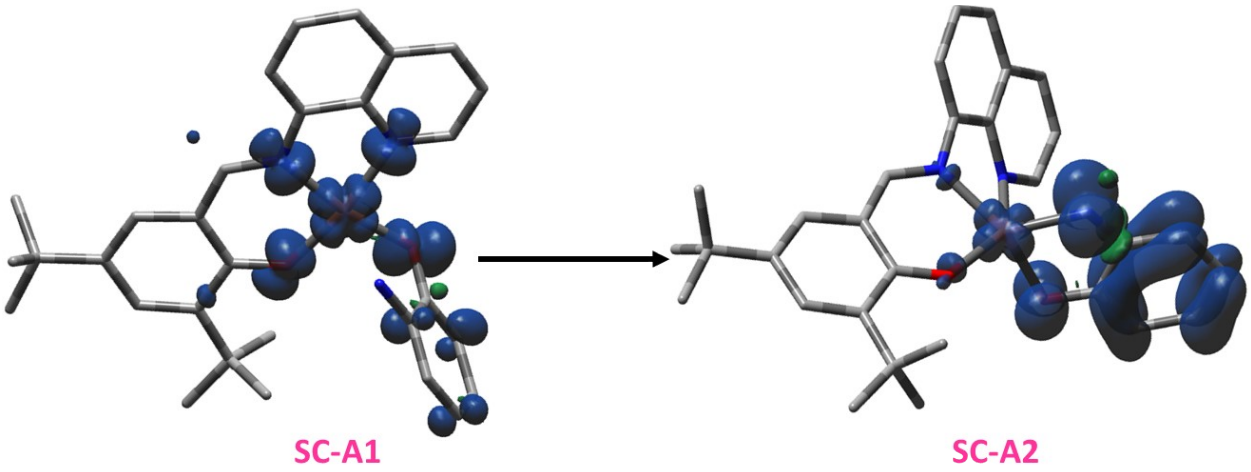

Figure S21: Spin density of the intermediates **SC-A1** and **SC-A2** for phenoxazinone synthase activity.

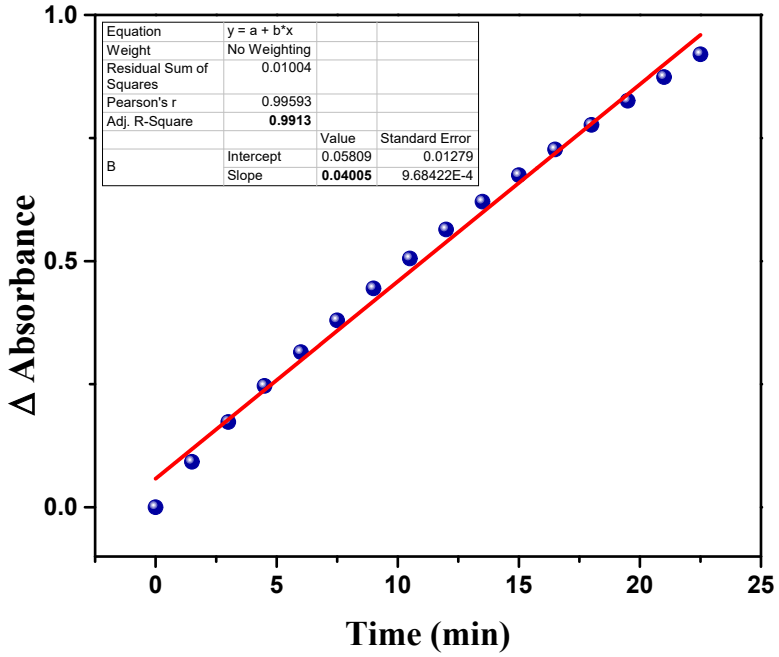

Figure S22: Δ*A* (change in absorbance at 400 nm) vs. *t* (time) plot of the catalytic oxidation of 3,5-DTBC by complexes **1.**

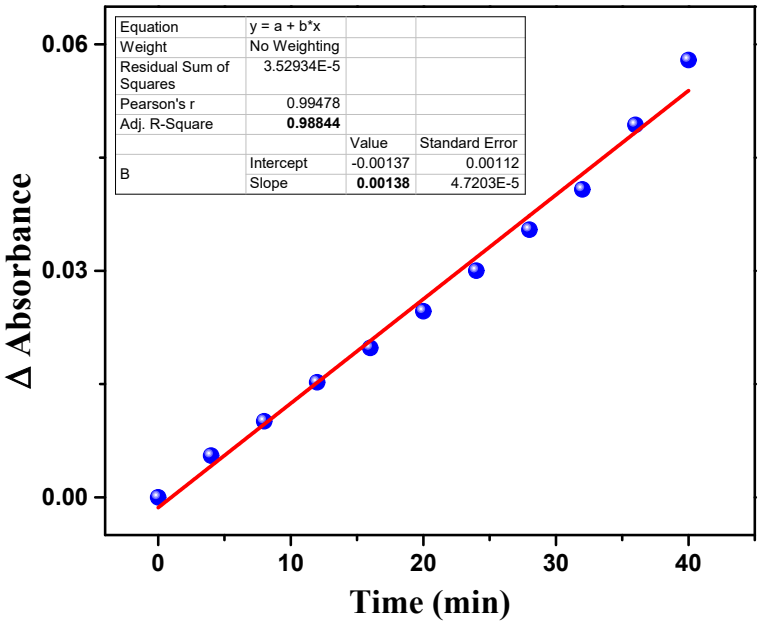

Figure S23: Δ*A* (change in absorbance at 436 nm) vs. *t* (time) plot of the catalytic oxidation of OAPH by complexes **1.**

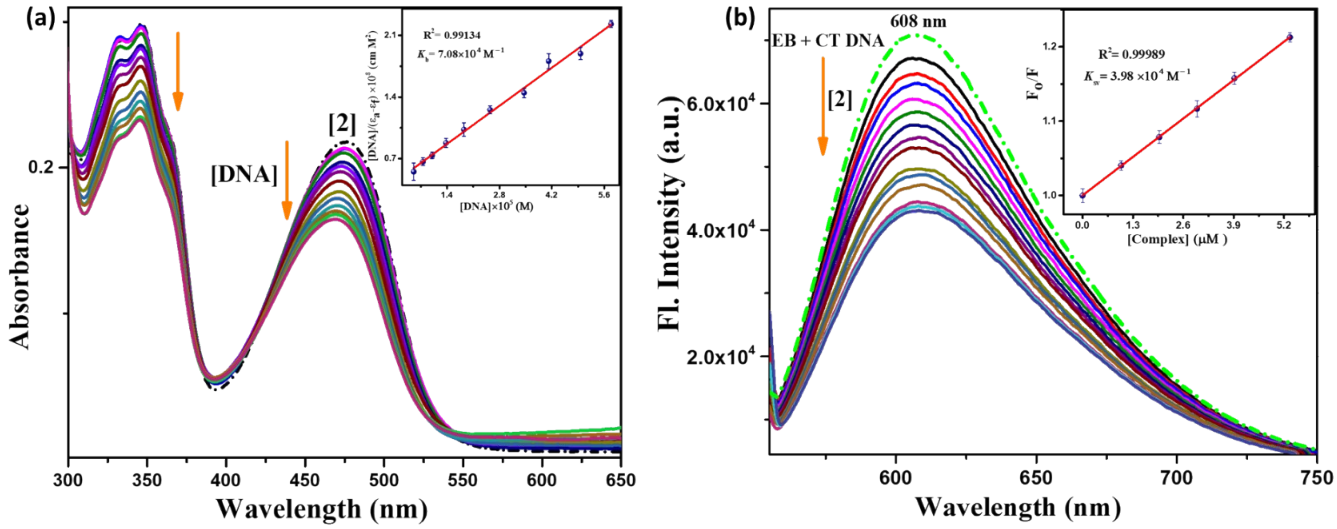

Figure S24: (a) Absorption spectral titration of complex-**2** [1.3×10^{-5} (M)] with gradual addition of CT DNA in Tris-HCl/NaCl buffer; Inset: Plot of $\frac{[DNA]}{(\varepsilon_a - \varepsilon_f)}$ versus [DNA]. (b) Fluorescence quenching titration using complex-**2**, [EB] = 15 μM, [DNA] = 30 μM, Inset: Stern Volmer quenching plot.

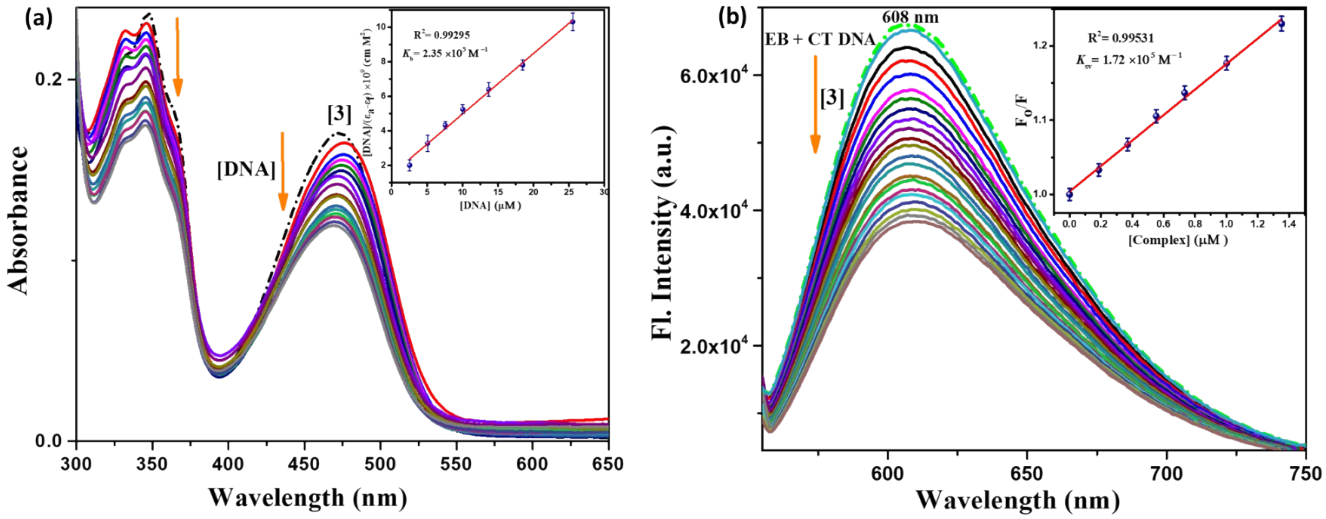

Figure S25: (a) Absorption spectral titration of complex-**3** [0.80×10^{-5} (M)] with gradual addition of CT DNA in Tris-HCl/NaCl buffer; Inset: Plot of $\frac{[DNA]}{(\varepsilon_a - \varepsilon_f)}$ versus [DNA]. (b) Fluorescence

quenching titration using complex-**3**, [EB] = 15 μM, [DNA] = 30 μM, Inset: Stern Volmer quenching plot.

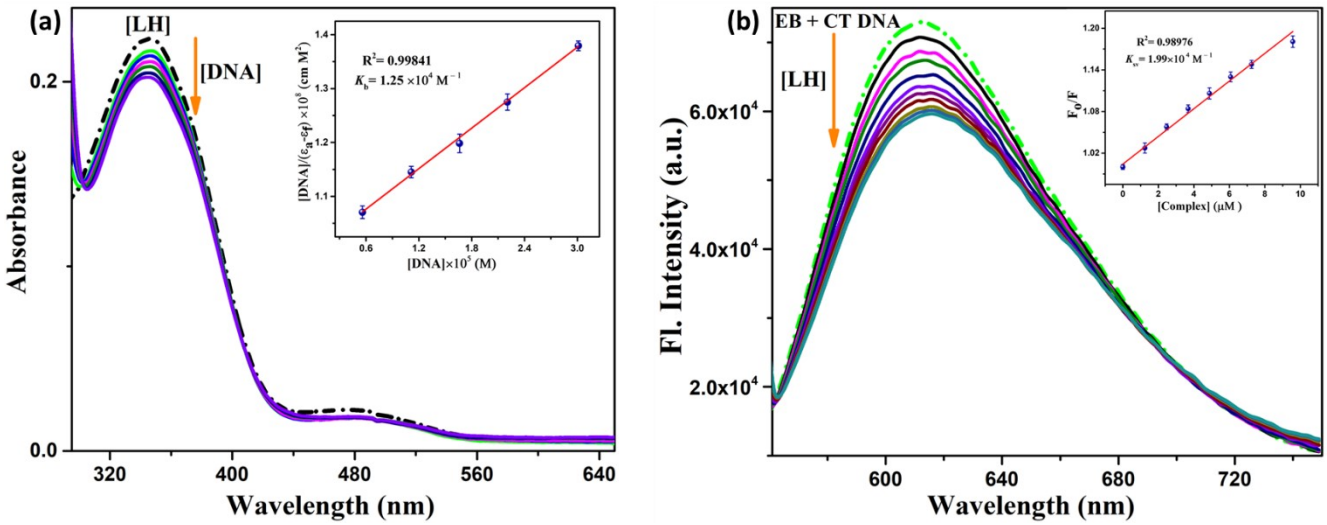

Figure S26: DNA binding study with free ligand **LH**; (a) Absorption spectral titration, (b) Fluorescence quenching titration.

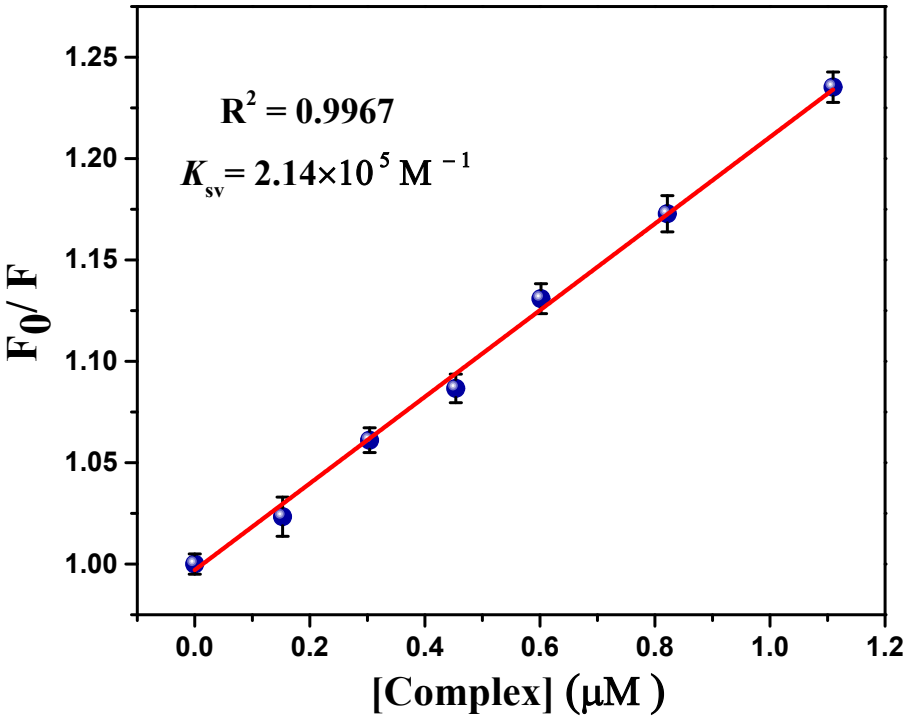

Figure S27: Stern Volmer quenching plot of BSA fluorescence by complex **1**

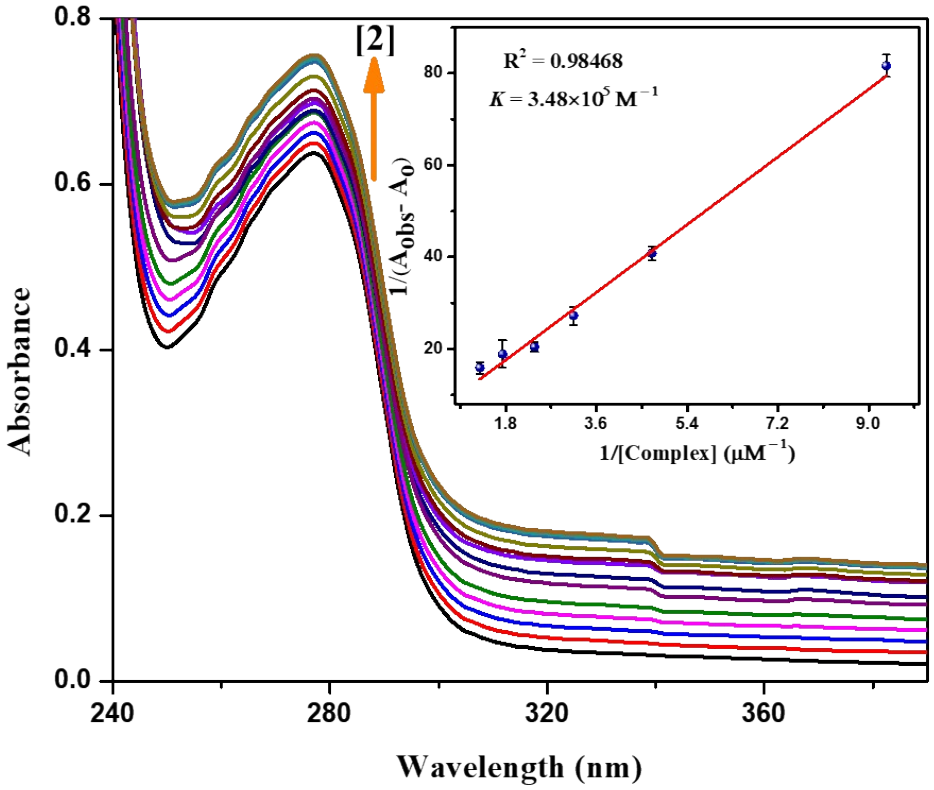

Figure S28: Absorption spectral titration of BSA (10 μM in phosphate-buffer solution) upon gradual addition of complex **2**. Insets: $1/(A_{obs} - A_0)$ vs. 1/[complex] plots of BSA absorption titration.

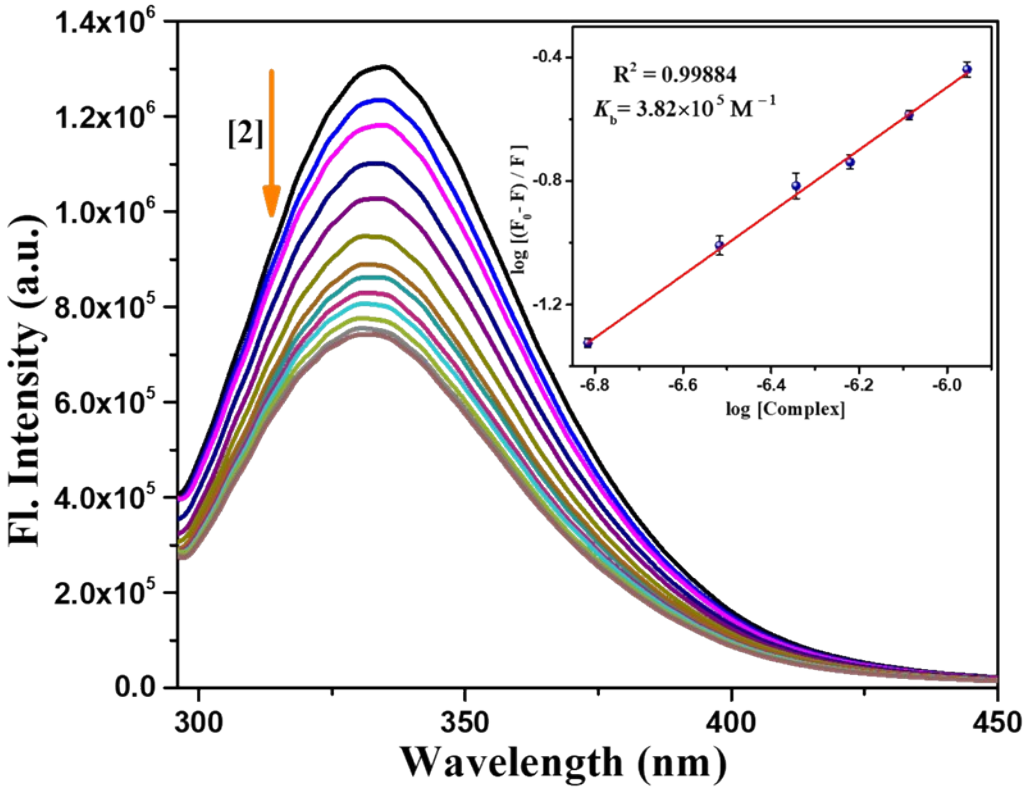

Figure S29: Fluorescence quenching titration of BSA (10 μM in phosphate-buffer solution) upon gradual addition of complex **2**. Insets: Scatchard plots of the BSA fluorescence quenching titration using complex **2**.

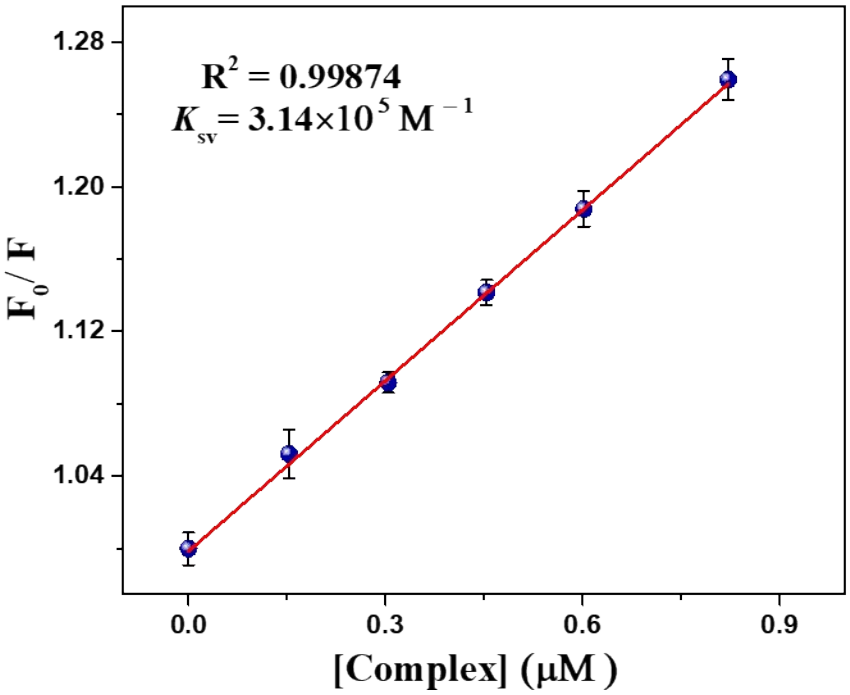

Figure S30: Stern Volmer quenching plot of BSA using complex **2**

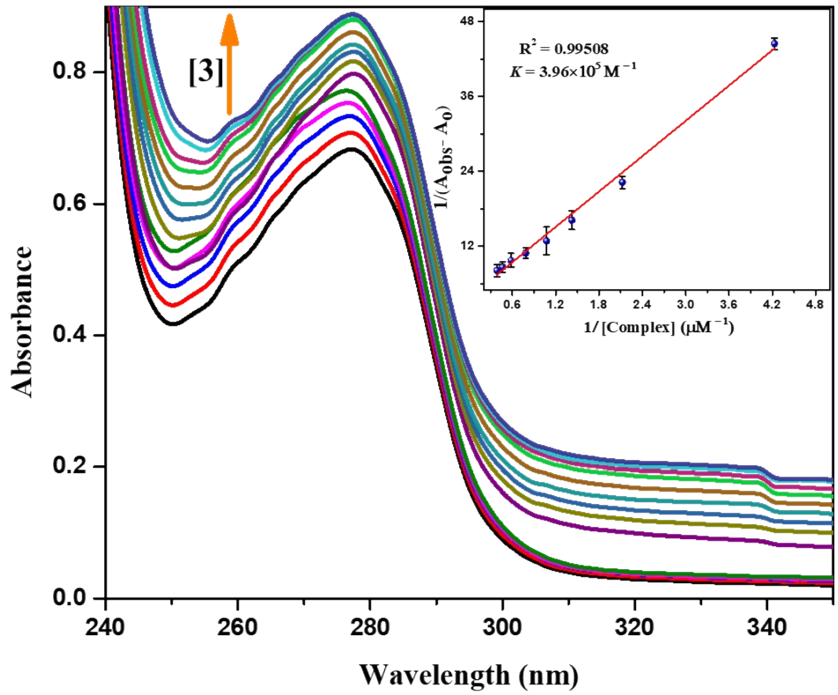

Figure S31: Absorption spectral titration of BSA (10 μM in phosphate-buffer solution) upon gradual addition of complex **3**. Insets: $1/(A_{obs} - A_0)$ vs. 1/[complex] plots of BSA absorption titration.

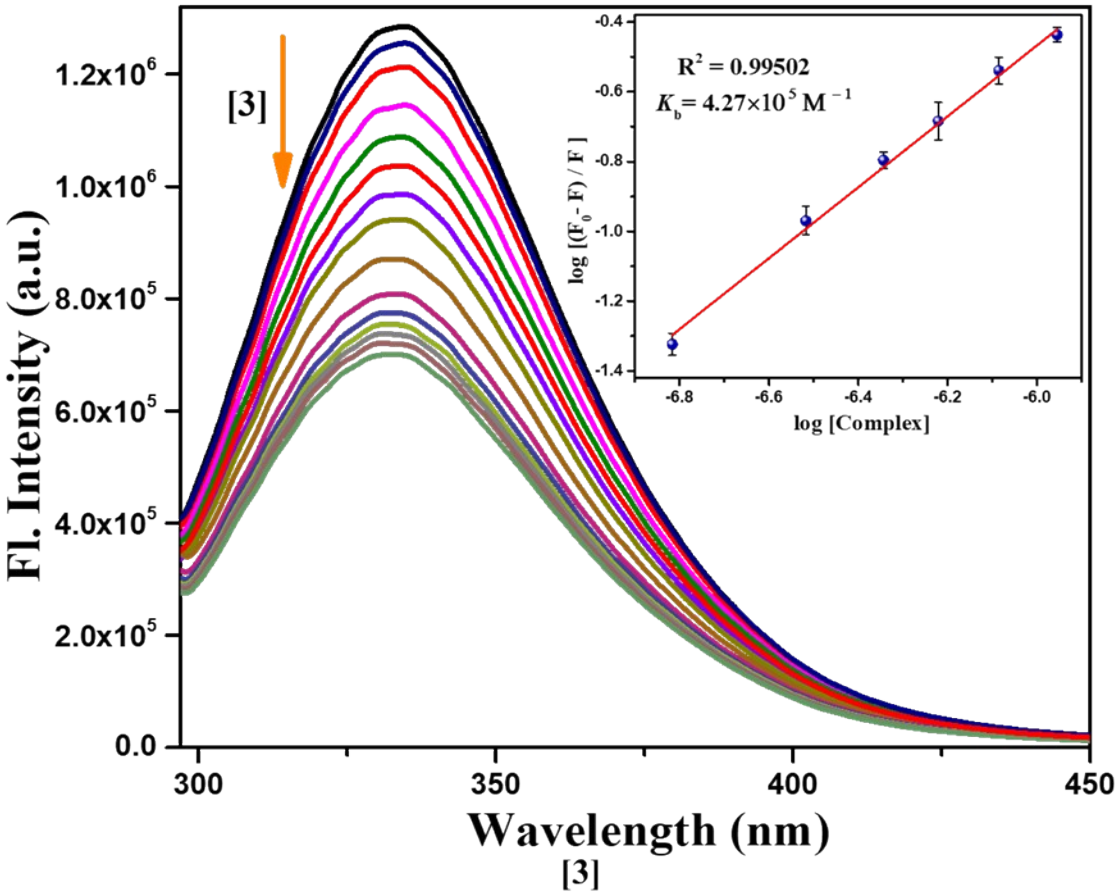

Figure S32: Fluorescence quenching titration of BSA (10 μM in phosphate-buffer solution) upon gradual addition of complex **3**. Insets: Scatchard plots of the BSA fluorescence quenching titration using complex **3**.

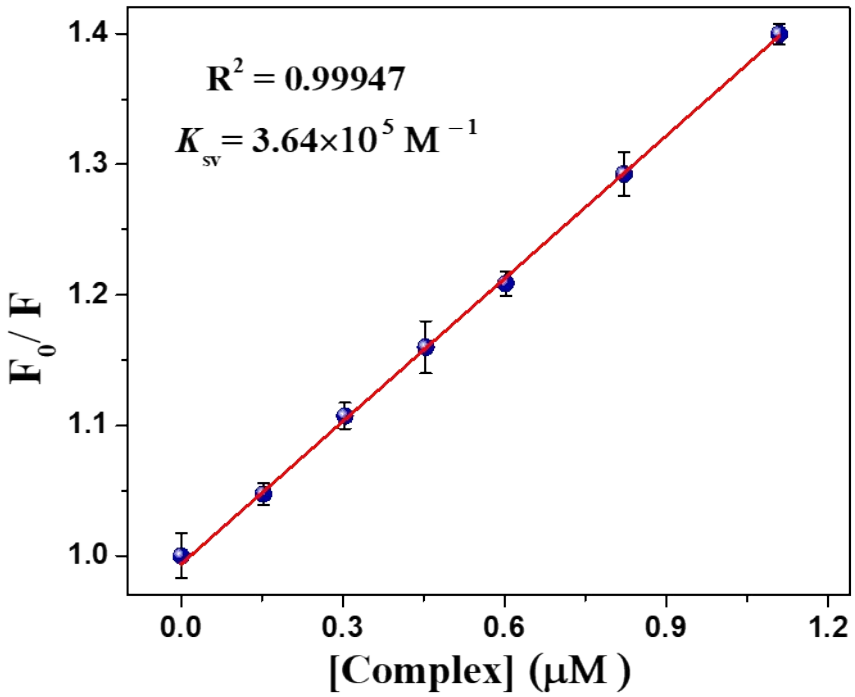

Figure S33: Stern Volmer quenching plot of BSA using complex **3**

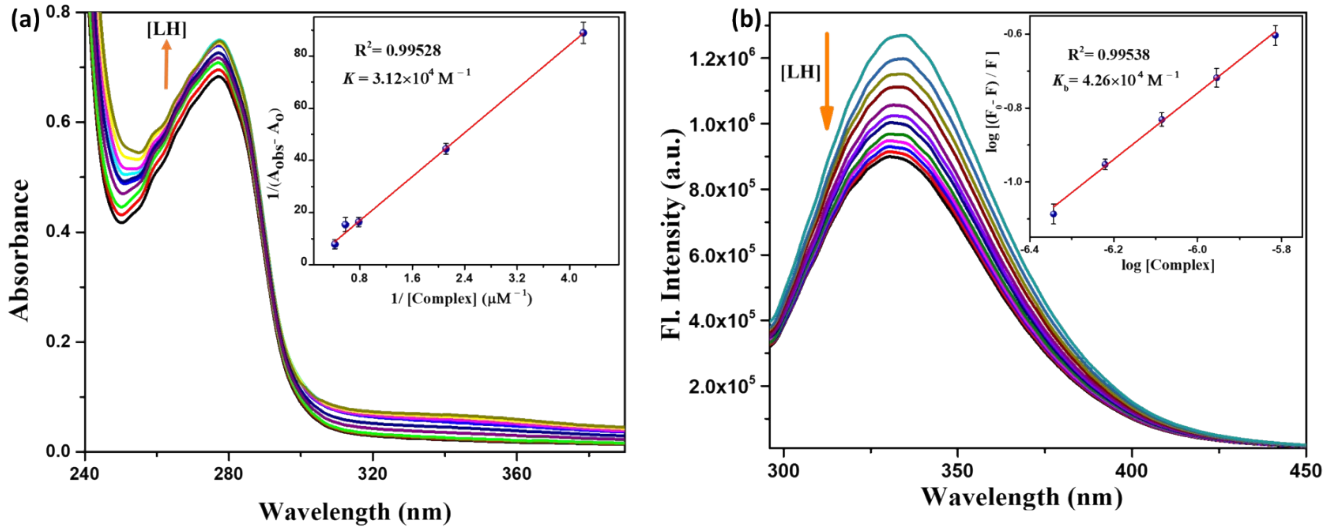

Figure S34: (a) Absorption spectral titration (b) Fluorescence quenching titration of BSA (in phosphate-buffer solution) upon gradual addition of ligand (**LH**); Insets: (a)$1/(A_{obs} - A_0)$ vs. 1/[complex] plots of absorption titration, (b) Scatchard plots of fluorescence quenching titration of BSA.

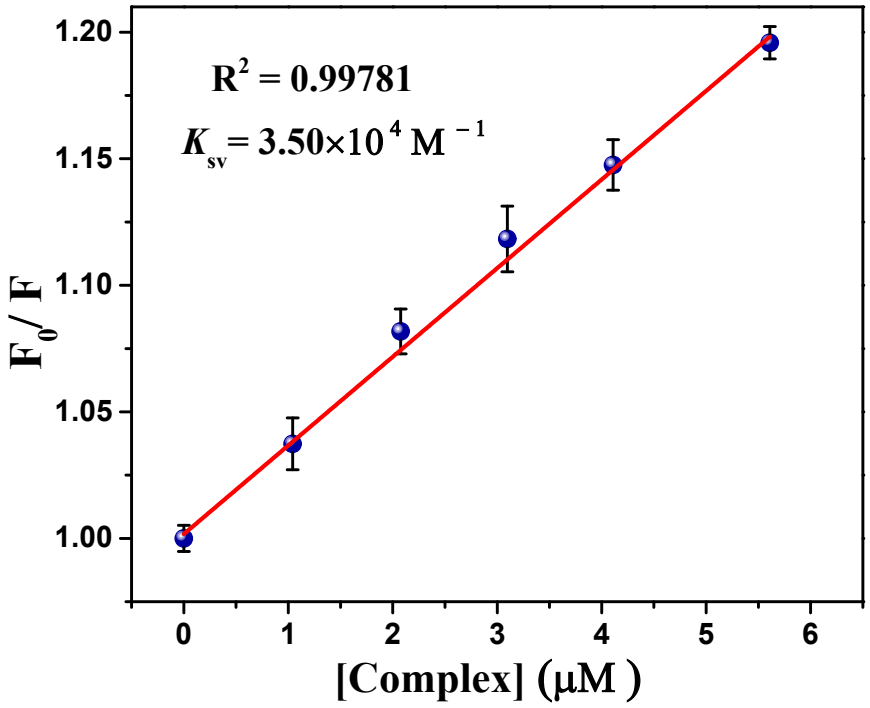

Figure S35: Stern Volmer quenching plot of BSA using ligand (**LH**)

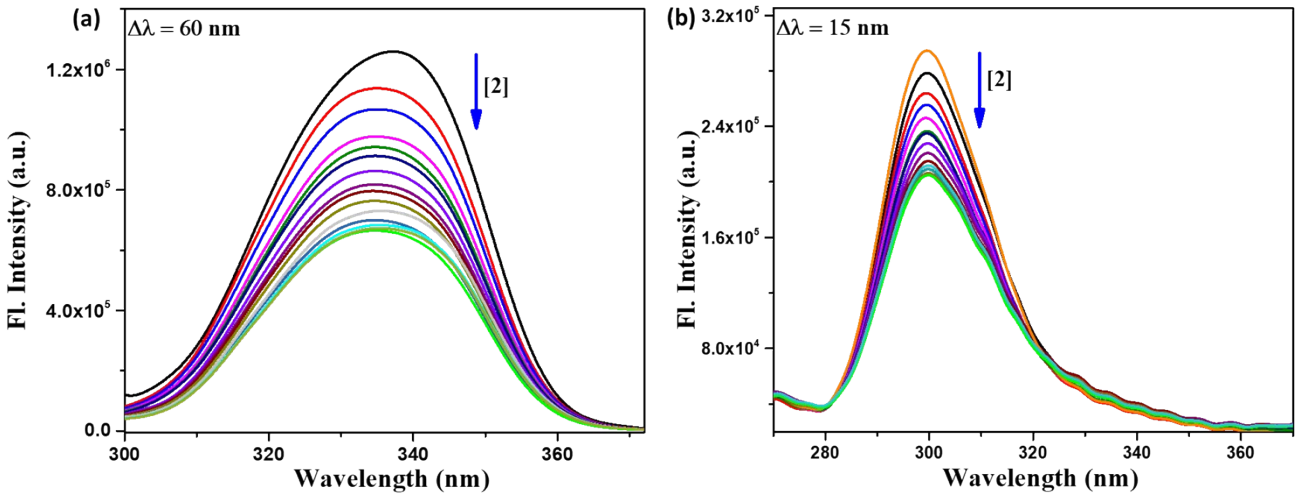

Figure S36: Synchronous fluorescence spectral titration of BSA using complex **2** employing (a) Δλ = 60nm, specific for Tryptophan moiety of BSA and (b) Δλ = 15 nm, specific for Tyrosine moiety of BSA.

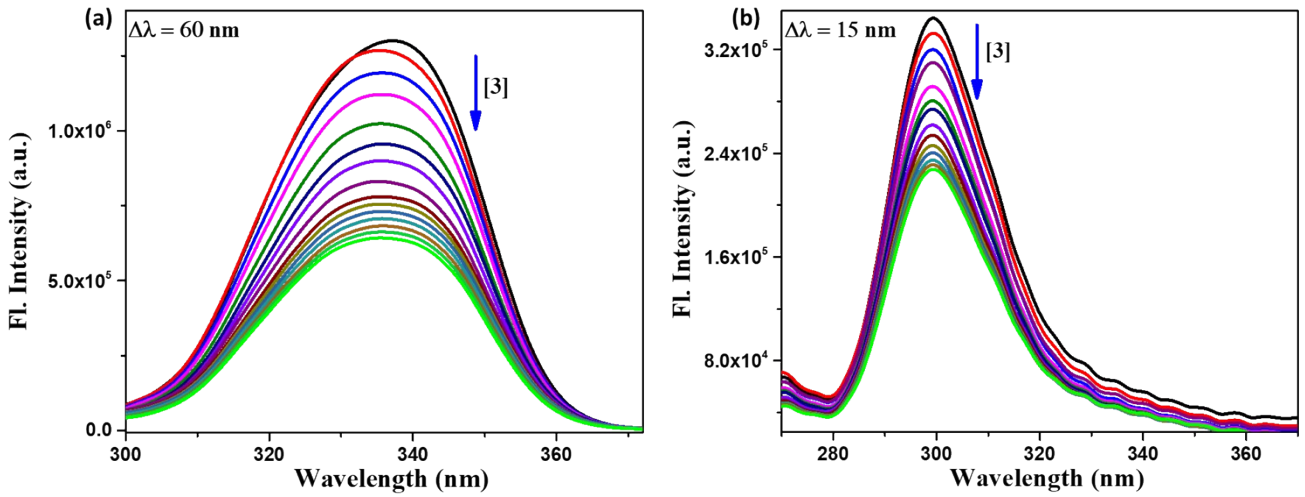

Figure S37: Synchronous fluorescence spectral titration of BSA using complex **3** employing (a) Δλ = 60nm, specific for Tryptophan moiety of BSA and (b) Δλ = 15 nm, specific for Tyrosine moiety of BSA.

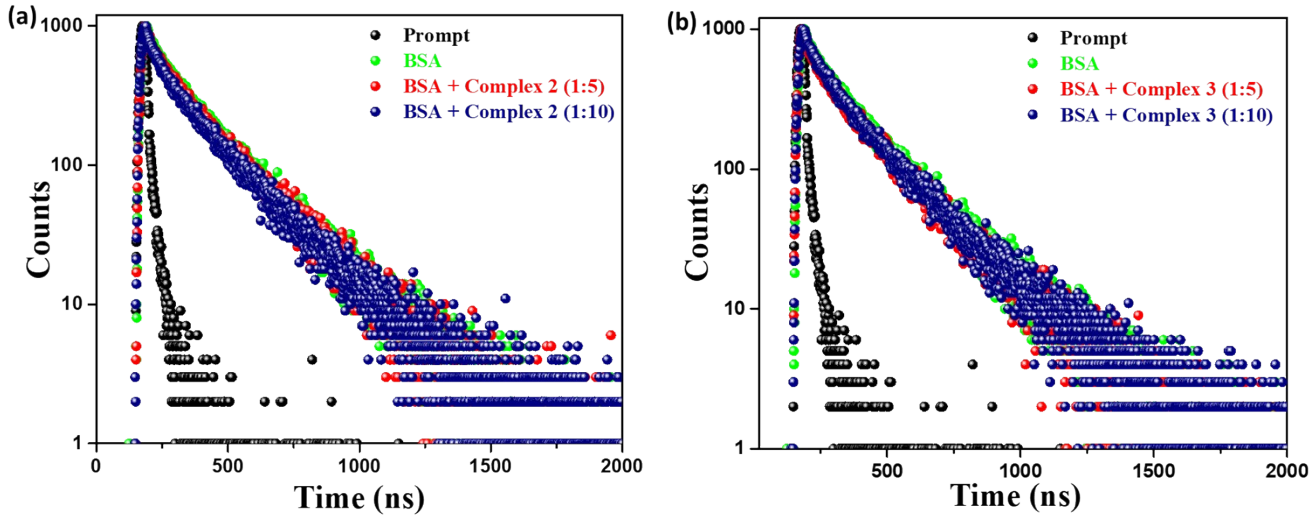

Figure S38: Time resolved fluorescence lifetime titration of BSA (1μM) using (a) complex **2** and (b) complex **3**.

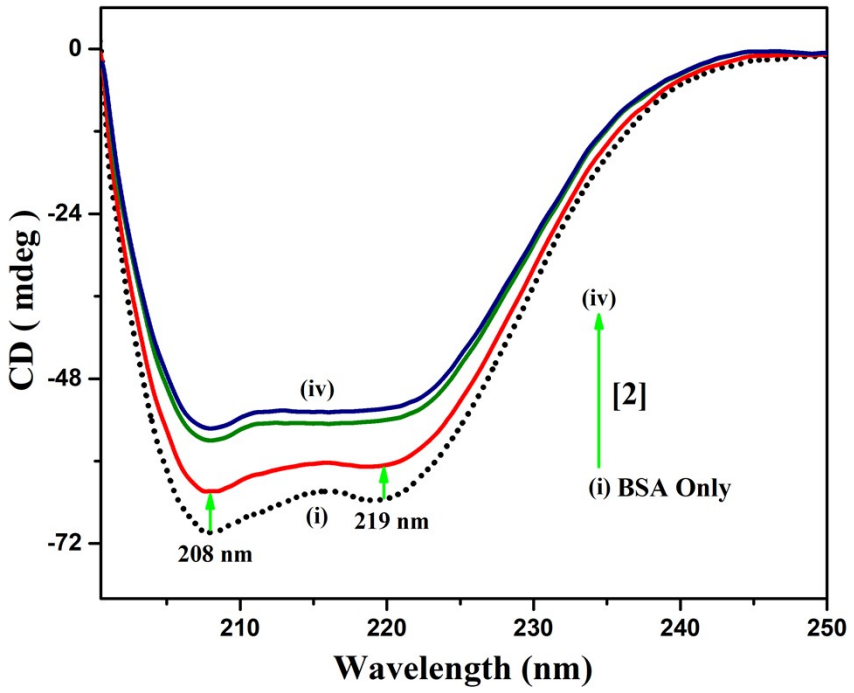

Figure S39: CD spectrum of BSA with different molar ratios of complex **2**.

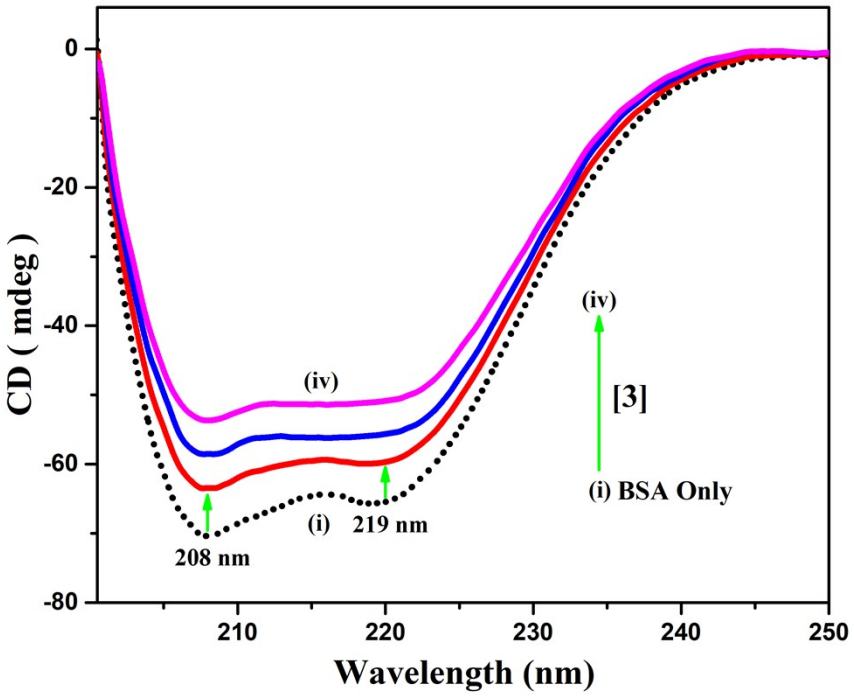

Figure S40: CD spectrum of BSA with different molar ratios of complex **3**.

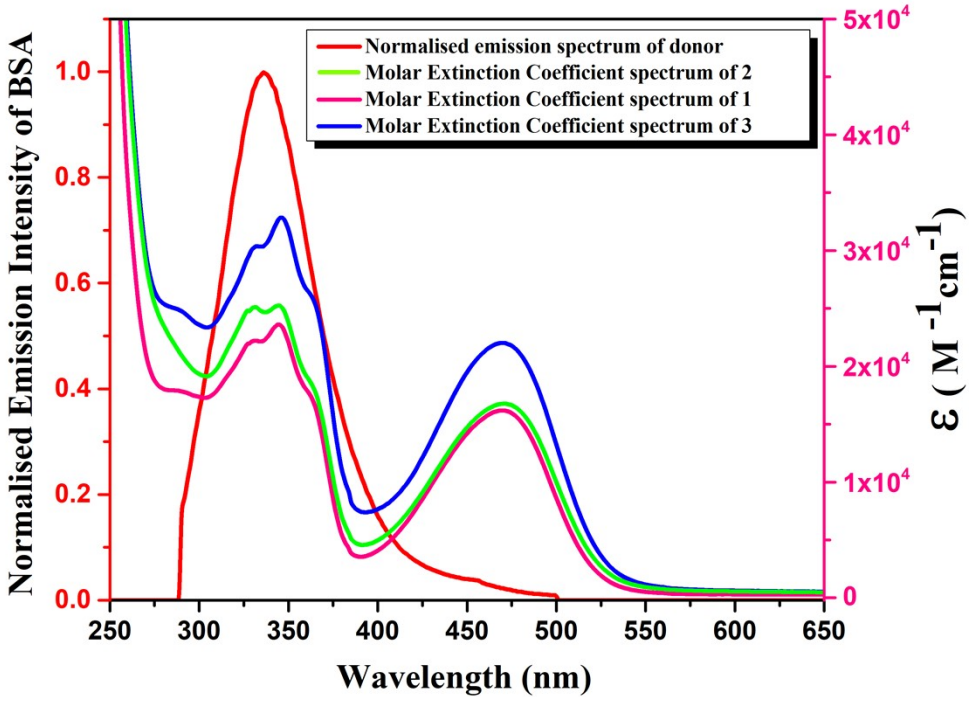

Figure S41: Spectral overlap of Normalized emission spectrum of BSA in PBS buffer (donor) with molar extinction coefficient of complex **1**, **2** and **3** in DMSO (acceptor).

References

1. J. C. Duff *J. Chem. Soc.*, 1941, 547-550
2. (a) Q.-s. Shi, X. Hao, C. Redshaw and W.-h. Sun, *Chin. J. Polym. Sci.*, 2013, **31**, 769-777; (b) F. da S. Gomes, A. L. Bergamo and O. de L. Casagrande Jr, *Macromol. Chem. Phys.*, 2014, **215**, 1735-1743.
3. L. Farrugia, *J. Appl. Cryst.*, 2012, **45**, 849-854.
4. (a) G. Sheldrick, *Acta Cryst.*, 2008, A**64**, 112-122; (b) G. Sheldrick, *Acta Cryst.,* 2015, C**71**, 3-8.
5. SMART and SAINT, Area Detector Software Package and SAX Area Detector Integration Program; Bruker Analytical X-Ray; 1997, Madison, WI, USA.
6. G. M. Sheldrick, *Sadabs*, 1996.
7. L. Farrugia, *J. Appl. Cryst.*, 1997, **30**, 565.
8. M.J.Frisch,G.W.Trucks,H.B.Schlegel,G.E.Scuseria,M.A. Robb,J.R.Cheeseman, G. Scalmani, V. Barone, B. Mennucci, G.A. Petersson, H. Nakatsuji, M. Caricato, X. Li, H.P. Hratchian, A.F. Izmaylov, J. Bloino, G. Zheng, J.L. Sonnenberg, M. Hada, M. Ehara, K. Toyota, R. Fukuda, J. Hasegawa, M. Ishida, T. Nakajima, Y. Honda, O. Kitao, H. Nakai, T. Vreven, J.A. Montgomery Jr., J.E. Peralta, F. Ogliaro, M. Bearpark, J.J. Heyd, E. Brothers, K.N. Kudin, V.N. Staroverov, R. Kobayashi, J. Normand, K. Raghavachari, A. Rendell, J.C. Burant, S.S. Iyengar, J. Tomasi, M. Cossi, N. Rega, J.M. Millam, M. Klene,

J.E. Knox, J.B. Cross, V. Bakken, C. Adamo, J. Jaramillo, R. Gomperts, R.E. Stratmann, O. Yazyev, A.J. Austin, R. Cammi, C. Pomelli, J.W. Ochterski, R.L. Martin, K. Morokuma, V.G. Zakrzewski, G.A. Voth,P. Salvador, J.J. Dannenberg, S. Dapprich, A.D. Daniels, Ö. Farkas, J.B. Foresman, J.V. Ortiz, J. Cioslowski, D.J. Fox, Gaussian 09, Revision D.01, Gaussian Inc, Wallingford CT, 2009.

9. Dennington, R., Keith, T., Millam, J. GaussView, Version 5.0.8.: Semichem Inc., Shawnee Mission KS; 2009.
10. (a) A. D. Becke, *J. Chem. Phys.*, 1993, **98**, 5648-5652; (b) C. Lee, W. Yang and R. G. Parr, *Phys. Rev. B*, 1988, **37**, 785-789.
11. (a) P. J. Hay and W. R. Wadt, *J. Chem. Phys.,*1985, **82**, 270-283; (b) W. R. Wadt and P. J. Hay, *J. Chem. Phys.,*1985, **82**, 284-298; (c) P. J. Hay and W. R. Wadt, *J. Chem. Phys.,* 1985, **82**, 299-310.
12. (a) R. Bauernschmitt and R. Ahlrichs, *Chem. Phys. Lett.*, 1996, **256**, 454-464; (b) R. E. Stratmann, G. E. Scuseria and M. J. Frisch, *J. Chem. Phys.*, 1998, **109**, 8218-8224; (c) M. E. Casida, C. Jamorski, K. C. Casida and D. R. Salahub, *J. Chem. Phys.*, 1998, **108**, 4439-4449.
13. (a) V. Barone and M. Cossi, *J. Phys. Chem. A*, 1998, **102**, 1995-2001; (b) M. Cossi and V. Barone, *J. Chem. Phys.*, 2001, **115**, 4708-4717; (c) M. Cossi, N. Rega, G. Scalmani and V. Barone, *J. Comput. Chem.*, 2003, **24**, 669-681
14. N. M. O'Boyle, A. L. Tenderholt and K. M. Langner, *J. Comput. Chem.,* 2008, **29**, 839-845.
15. (a) M. A. Spackman and D. Jayatilaka, *CrystEngComm*, 2009, **11**, 19-32; (b) F. L. Hirshfeld, *Theor. Chem. Acc.,*1977, **44**, 129-138; (c) H. F. Clausen, M. S. Chevallier, M. A. Spackman and B. B. Iversen, *New J. Chem.*, 2010, **34**, 193-199.
16. (a) A. L. Rohl, M. Moret, W. Kaminsky, K. Claborn, J. J. McKinnon and B. Kahr, *Cryst. Growth Des.*, 2008, **8**, 4517-4525; (b) A. Parkin, G. Barr, W. Dong, C. J. Gilmore, D. Jayatilaka, J. J. McKinnon, M. A. Spackman and C. C. Wilson, *CrystEngComm*, 2007, **9**, 648-652; (c) M. A. Spackman and J. J. McKinnon, *CrystEngComm*, 2002, **4**, 378-392.
17. (a) C. F. Mackenzie, P. R. Spackman, D. Jayatilaka and M. A. Spackman, *IUCrJ*, 2017, **4**, 575-587; (b) P. R. Spackman, M. J. Turner, J. J. McKinnon, S. K. Wolff, D. J. Grimwood, D. Jayatilaka and M. A. Spackman, *J. Appl. Crystallogr.*, 2021, **54**, 1006-1011.
18. N. Sarkar, K. Harms and S. Chattopadhyay, *Polyhedron*, 2018, **141**, 198-207.
19. (a) S. K. Dey and A. Mukherjee *New J. Chem.*, 2014, **38**, 4985-4995; (b) E. Monzani, L. Quinti, A. Perotti, L. Casella, M. Gullotti, L. Randaccio, S. Geremia, G. Nardin, P. Faleschini and G. Tabbì, *Inorg. Chem.*, 1998, **37**, 553-562; (c) A. Das, K. Bhattacharya, L. K. Das, S. Giri and A. Ghosh, *Dalton Trans.*, 2020, **49**, 3369-3371; (d) N. Podder and S. Mandal, *New J. Chem.*, 2020, **44**, 12793-12805
20. (a) S. Mahato, N. Meheta, M. Kotakonda, M. Joshi, P. Ghosh, M. Shit, A. R. Choudhury and B. Biswas, *Appl. Organomet. Chem.*, 2020, **34**, e5935; (b) P. K. Mudi, R. K. Mahato, M. Joshi, M. Shit, A. R. Choudhury, H. S. Das and B. Biswas, *Appl. Organomet. Chem.*, 2021, **35**, e6211; (c) P. Adak, B. Ghosh, A. Bauzá, A. Frontera, A. J. Blake, M. Corbella, C. Das Mukhopadhyay and S. K. Chattopadhyay, *RSC Adv.*, 2016, **6**, 86851-86861.

21. M. E. Reichmann, S. A. Rice, C. A. Thomas and P. Doty, *J. Am. Chem. Soc.*, 1954, **76**, 3047-3053.
22. R. Bellam, D. Jaganyi, A. Mambanda, R. Robinson and M. D. BalaKumaran, *RSC Adv.*, 2019, **9**, 31877-31894.
23. (a) M. Kumar, G. Kumar, N. K. Mogha, R. Jain, F. Hussain and D. T. Masram, *Spectrochim. Acta*, 2019, **212**, 94–104; (b) M. Kumar, N. K. Mogha, G. Kumar, F. Hussain and D. T. Masram, *Inorg. Chim. Acta*, 2019, **490**, 144–154.
24. S. Tunç, A. Çetinkaya and O. Duman, *J. Photochem. Photobiol. B: Biol.*, 2013, **120**, 59-65.
25. T. A. Wani, A. H. Bakheit, S. Zargar, M. A. Hamidaddin and I. A. Darwish, *PLOS ONE*, 2017, **12**, e0176015.
26. (a) M. Kumar, G. Kumar, K. M. dadure and D. T. Masram, *New J. Chem*., 2019, **43**, 15462–15481; (c) S. Afrin, Y. Rahman, M. Alhaji Isa, S. Ahmed, M. Tabish, *J. Biomol. Struct. Dyn.*, 2020, **38**, 1375-1387.
27. H. Gao, L. Lei, J. Liu, Q. Kong, X. Chen and Z. Hu, *J. Photochem. Photobiol., A*, 2004, **167**, 213–221.
28. A. Banerjee, M. Mohanty, S. Lima, R. Samanta, E. Garribba, T. Sasamori and R. Dinda, *New J. Chem.,* 2020, **44**, 10946-10963.
29. S. U. Parsekar, P. Velankanni, S. Sridhar, P. Haldar, N. A. Mate, A. Banerjee, P. K. Sudhadevi Antharjanam, A. P. Koley and M. Kumar, *Dalton Trans.,* 2020, **49**, 2947-2965.
30. (a) S. Dolai, K. Das, A. Bhunia, V. Bertolasi and S. C. Manna, *Appl. Organomet. Chem.*, 2018, **32**, e4506; (b) J. Reim, B. Krebs, J. Chem. Soc. Dalton Trans. 1997, 3793; (c) A. Bhunia, P. Vojtíšek, V. Bertolasi, S. C. Manna, *J. Mol. Struct.*, 2019, **1189**, 94-101; (d) T. P. Camargo, R. A. Peralta, R. Moreira, E. E. Castellano, A. J. Bortoluzzi and A. Neves, *Inorg. Chem. Commun.*, 2013, **37**, 34-38; (e) A. Bhunia, P. Vojtíšek and S. C. Manna, *J. Mol. Struct.*, 2019, **1179**, 558-567.
31. T. Dutta, S. Mirdya, P. Giri and S. Chattopadhyay, *Polyhedron*, 2020, **175**, 114164.

.